Remote Sensing of Environment 127 (2012) 298–315

Contents lists available at SciVerse ScienceDirect

Remote Sensing of Environment

journal homepage: www.elsevier.com/locate/rse

Carotenoid content estimation in a heterogeneous conifer forest using narrow-band indices and PROSPECT + DART simulations

Rocío Hernández-Clemente [a,*], Rafael M. Navarro-Cerrillo [a], Pablo J. Zarco-Tejada [b]

[a] E.T.S.I.A.M.-Dpto. de Ingeniería Forestal, Universidad de Córdoba, Campus de Rabanales, 14071 Córdoba, Spain

[b] Instituto de Agricultura Sostenible (IAS), Consejo Superior de Investigaciones Científicas (CSIC), Alameda del Obispo, s/n, 14004 Córdoba, Spain

ARTICLE INFO

Article history:
Received 19 January 2012
Received in revised form 17 August 2012
Accepted 12 September 2012
Available online xxxx

Keywords:
Narrow-band indices
Carotenoids
R_{515}/R_{570}
Radiative transfer
Airborne remote sensing
UAV
Heterogeneous conifer forest

ABSTRACT

The present study explored the use of narrow-band indices formulated in the visible spectral region at leaf and canopy levels to estimate carotenoid content. The research area was a pine forest affected by decline processes. Spectral reflectance and pigment content including chlorophylls *a* and *b* ($Ca+b$), carotenoid ($Cx+c$) and xanthophyll cycle pigments (*VAZ*) were measured in needles for two consecutive years. The study was conducted using radiative transfer modeling methods and high-resolution airborne imagery acquired at 10 nm FWHM bandwidth. Airborne data consisted of high spatial resolution imagery acquired with a narrow-band multispectral camera on board an unmanned aerial vehicle (UAV). The imagery had 50 cm resolution and six spectral bands in the 500–800 nm range, enabling the identification of pure crowns to obtain the reflectance of individual trees. The indices evaluated were traditional formulations and new simple ratios developed by combining bands sensitive to $Cx+c$ absorption in the 500–600 nm region. The PROSPECT-5 model was coupled with the Discrete Anisotropic Radiative Transfer (DART) model to explore the performance of $Cx+c$-sensitive vegetation indices at leaf and canopy levels. The sensitivity of these indices to structural effects was assessed to study the potential scaling-up of $Cx+c$-related vegetation indices on heterogeneous canopies. Coefficients of determination between $Cx+c$ content and narrow-band vegetation indices revealed that traditional indices were highly related with $Cx+c$ content at leaf level ($r^2>0.90$; $P<0.001$ for the CRI index $(1/R_{515})-(1/R_{550})$) but highly affected by structural parameters at crown level ($r^2>0.44$; $P<0.001$). A new simple-ratio vegetation index proposed in this study (R_{515}/R_{570}) was found to be significantly related with $Cx+c$ content both at leaf ($r^2>0.72$; $P<0.001$) and canopy levels ($r^2>0.71$; $P<0.001$). Remote sensing cameras on board UAV platforms can provide very high multispectral and hyperspectral imagery for mapping biochemical constituents in heterogeneous forest canopies. This study demonstrates the feasibility of mapping carotenoid content to assess the physiological condition of forests.

1. Introduction

Carotenoid and chlorophyll pigment content provide valuable information about the physiological status of plants (Demmig-Adams & Adams, 1992). Chlorophylls – C_a and C_b – are essential pigments to absorb the energy of light and convert it to store chemical energy (Carter, 1994; Lichtenhaler, 1998). Total carotenoid pigments ($Cx+c$) (xanthophylls and carotenes) are usually represented by two (α- and β-) carotenes and five xanthophylls (lutein, zeaxanthin, violaxanthin, antheraxanthin and neoxanthin) (Demmig-Adams & Adams, 1992). Carotenoids have several physiological functions associated with photosynthesis, including a structural role in the organization of photosynthetic membranes, participation in light harvesting and energy transfer (Frank & Cogdell, 1996; Ritz et al., 2000), as well as quenching of $Ca+b$ excited state and photoprotection (Demmig-Adams & Adams, 1996; Thayer & Björkman, 1990; Young & Britton, 1990). Carotenoid content is known to be correlated with plant stress and photosynthetic capacity. For example, it has been observed that some carotenoids increase under high irradiance levels and high temperature environments (Kirchgebner et al., 2003) or at the onset of leaf senescence (Munné-Bosch & Peñuelas, 2003; Peñuelas et al., 1994). Some xanthophylls have been found to be involved in the non-photochemical quenching of chlorophyll fluorescence (CF), an important photoprotective process (Demmig-Adams & Adams, 1992). The xanthophylls involved in this process dissipate excess energy. This is commonly referred to as the xanthophyll cycle (Young et al., 1997).

The photoprotection system plays a critical role in plants adapted to the Mediterranean climate (Faria et al., 1996; Hernández-Clemente et al., 2011) because many Mediterranean environments are associated with high summer temperatures, high irradiation levels and drought. Thus, leaf pigment content has considerable importance as

* Corresponding author at: Dpto. Ingeniería Forestal, E.T.S.I.A.M. Universidad de Córdoba, Campus de Rabanales, Crta. N-IV km. 396, C.P. 14071; Córdoba, Spain. Tel.: +34 957218657; fax: +34 957212095.
E-mail address: rociohc@uco.es (R. Hernández-Clemente).
URL: http://www.treesat.com (R. Hernández-Clemente).

0034-4257/$ – see front matter
http://dx.doi.org/10.1016/j.rse.2012.09.014

a physiological indicator of plant growth and stress in the Mediterranean forest.

Recent studies have focused on retrieving leaf pigment content from remote sensing data (Malenovsky et al., 2007; Meggio et al., 2008; Wu et al., 2008; Zarco-Tejada et al., 2004). Nevertheless, the overlapping absorption exhibited by chlorophyll and carotenoids in the visible region makes it difficult to retrieve $Ca+b$ and $Cx+c$ content independently (Feret et al., 2011). Several studies have successfully estimated $Ca+b$ for chlorosis detection in vegetation using visible ratios (Datt, 1998), visible/NIR ratios (Gitelson et al., 2003, 2006; Haboudane et al., 2002), red edge reflectance-ratio indices (Carter & Spiering, 2002; Gitelson et al., 2003; le Maire et al., 2004; Richardson & Berlyn, 2002; Sims & Gamon, 2002), spectral and derivative red edge indices (Miller et al., 1990) and scaling-up and model inversion methods with narrow bands in forest canopies (Zarco-Tejada et al., 2001).

Most methods have focused on retrieving $Ca+b$ content (Main et al., 2011), but only a few studies have focused on estimating $Cx+c$ (Gitelson et al., 2002). In fact, research conducted at canopy level using high-resolution narrow-band imagery is very limited or nonexistent. Candidate $Cx+c$ optical indices have been grouped into two main categories based on the spectral region used: visible ratios (Gamon et al., 1992; Garrity et al., 2011; Gitelson et al., 2003, 2006; Hernández-Clemente et al., 2011) and visible/NIR ratios (Blackburn, 1998; Chappelle et al., 1992; Datt, 1998; Merzlyak et al., 1999; Peñuelas et al., 1995). Gitelson et al. (2002) developed indices within the visible region and showed that carotenoid absorption was related to a prominent spectral peak located at 520 nm corresponding to senescing and mature leaves. The same authors showed that the sensitivity of reciprocal reflectance to $Cx+c$ content was maximal in a spectral range around 510 nm, proposing the Carotenoid Content Index as $(1/R_{515})-(1/R_{550})$ and $(1/R_{515})-(1/R_{700})$ (Gitelson et al., 2002). The 550 and 700 nm reflectance bands were used in their study to minimize the effect of chlorophylls in this spectral range. In other studies, the Photochemical Reflectance Index (PRI) (Gamon et al., 1992), originally developed to estimate changes in the xanthophyll cycle pigments, has been successfully related to the $Cx+c/Ca+b$ ratio at leaf level (Garrity et al., 2011; Sims & Gamon, 2002). In particular, Garrity et al. (2011) found significant relationships between the $\mathrm{PRI}\cdot[(R_{760}/R_{700})^{-1}]$ and the $Cx+c/Ca+b$ ratio.

The main spectral bands proposed for $Cx+c$ estimation in the visible/NIR region are the following: i) combinations of bands around the 700 nm region (678, 708 and 760 nm) and bands in the green region (500, 550 nm) (Chappelle et al., 1992; Merzlyak et al., 1999); and ii) combinations of R_{800} with visible bands (470, 680, 635 nm) (Blackburn, 1998; Peñuelas et al., 1995). Chappelle et al. (1992) analyzed different ratios of leaf reflectance spectra to identify bands corresponding to the absorption of $Ca+b$ and $Cx+c$. They found that the $Cx+c$ fraction had a maximum absorption peak at 500 nm and proposed the R_{760}/R_{500} ratio as a quantitative measure of this pigment at leaf level. Successful scaling-up of such results to the canopy level required additional studies focused on the effects of the structure and background on the indices proposed for $Cx+c$ and $Ca+b$ estimation, such as the R_{750}/R_{710} index (Zarco-Tejada et al., 2001). Recent studies have demonstrated that hyperspectral indices for $Ca+b$ estimation in leaves cannot be readily applied to imagery due to the large structural effects present in heterogeneous canopies (Wu et al., 2008; Zarco-Tejada et al., 2004). In particular, Malenovsky et al. (2007) proposed a new optical index defined as the Area under curve Normalized to Maximal Band depth between 650 and 725 nm (ANMB 650–725) to estimate the chlorophyll concentration of a Norway spruce crown.

These scaling-up studies are even more important in forest canopies because bidirectional and background effects increase in conifer forests under sparse and open conditions (Zarco-Tejada et al., 2004). While some studies have used the inversion of physically based models (Malenovsky et al., 2008), others have used simple statistical relationships with a variety of optical spectral indices or combined empirical relationships coupled with radiative transfer simulation models (Broge & Leblanc, 2001; Gastellu-Etchegorry & Bruniquel-Pinel, 2001). With the development of PROSPECT-5 (Féret et al., 2008; Jacquemoud & Baret, 1990), it is possible to explore the validation of carotenoid content retrieval at leaf level in a wide number of species (Féret et al., 2011). At canopy level, models such as the 3-dimensional Discrete Anisotropic Radiative Transfer (DART) model (Gastellu-Etchegorry et al., 1996, 2004) can be used to model complex structures and canopy architectures to simulate coniferous canopies.

The simulation of forest canopy reflectance is used as well to perform sensitivity analyses of canopy structure, viewing geometry and background effects. An example is the assessment of physiological indices such as the PRI, which was found to be highly affected by background and structural variables (Hernández-Clemente et al., 2011; Suárez et al., 2009, 2008). Meggio et al. (2010) showed that $Cx+c$-related vegetation indices such as the Gitelson-$Cx+c$ index and the Gitelson-anthocyanin index were highly affected by canopy structure and soil background. In addition, Malenovsky et al. (2008) analyzed the effect of woody elements introduced into DART and

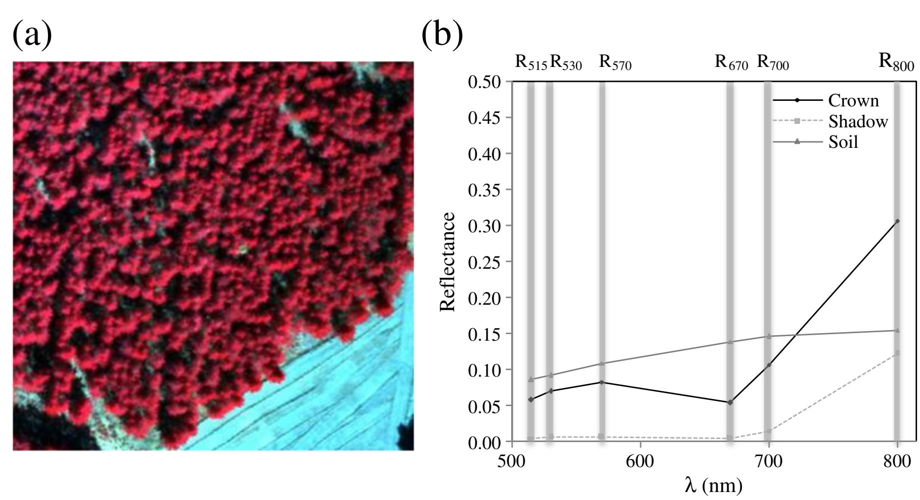

Fig. 1. (a) Example of imagery acquired with the high resolution narrow-band airborne multispectral camera on board the UAV platform; (b) spectral reflectance extracted from the imagery for pure tree crown, shadow and soil pixels.

Table 1
Hyperspectral vegetation and physiological indices proposed in other studies.

Index	Index ID	Formula	Reference	Scale
Leaf Area Index				
Normalized difference vegetation index	NDVI	$(R_{800}-R_{670})/(R_{800}+R_{670})$	Rouse et al. (1974)	Leaf/canopy
Chlorophyll estimation				
Structure insensitive pigment index	SIPI	$(R_{800}-R_{445})/(R_{800}+R_{680})$	Peñuelas et al. (1995)	Leaf
			Gitelson and Merzlyak (1996); Zarco-Tejada et al. (2004)	Leaf/canopy
Chlorophyll index red edge	$CI_{red\ edge}$	R_{750}/R_{710}	Haboudane, Miller, Tremblay, Zarco-Tejada, & Dextraze (2002); Meggio et al. (2010)	Leaf/canopy
Transformed Cab absorption in reflectance index	TCARI	$3*[(R_{700}-R_{670})-0.2*(R_{700}-R_{550})*(R_{700}/R_{670})$	Rondeaux et al. (1996); Meggio et al. (2010)	Leaf/canopy
Optimized soil-adjusted vegetation index	OSAVI	$(1+0.16)*(R_{800}-R_{670})/(R_{800}+R_{670}+0.16)$	Haboudane, Miller, Tremblay, Zarco-Tejada, & Dextraze (2002);	Leaf/canopy
	TCARI/OSAVI	$3*[(R_{700}-R_{670})-0.2*(R_{700}-R_{550})*(R_{700}/R_{670})/(1.16*(R_{800}-R_{670})/(R_{800}+R_{670}+0.16))$	Meggio et al. (2010)	Leaf/canopy
Carotenoid concentration				
Ratio analysis of reflectance spectra	RARS	R_{746}/R_{513}	Chappelle et al. (1992)	Leaf
Pigment-specific simple ratio	PSSRa	R_{800}/R_{680}	Blackburn (1998)	Leaf/canopy
Pigment-specific simple ratio	PSSRb	R_{800}/R_{635}	Blackburn (1998)	Leaf/canopy
Pigment-specific simple ratio	PSSRc	R_{800}/R_{470}	Blackburn (1998)	Leaf/canopy
Pigment-specific normalized difference	PSNDc	$(R_{800}-R_{470})/(R_{800}+R_{470})$	Blackburn (1998)	Leaf/canopy
Carotenoid concentration index	CRI_{550}	$(1/R_{515})-(1/R_{550})$	Gitelson et al. (2003, 2006)	Leaf
Carotenoid concentration index	CRI_{700}	$(1/R_{515})-(1/R_{700})$	Gitelson et al. (2003, 2006)	Leaf
Carotenoid concentration index	$RNIR^*CRI_{550}$	$(1/R_{510})-(1/R_{550})*R_{770}$	Gitelson et al. (2003, 2006)	Leaf
Carotenoid concentration index	$RNIR^*CRI_{700}$	$(1/R_{510})-(1/R_{700})*R_{770}$	Gitelson et al. (2003, 2006)	Leaf
Modified photochemical reflectance index	PRIm1	$(R_{515}-R_{530})/(R_{515}+R_{530})$	Hernández-Clemente et al. (2011)	Leaf/canopy
Photochemical reflectance index	PRI	$(R_{570}-R_{530})/(R_{570}+R_{530})$ $((R_{570}-R_{530})/(R_{570}+R_{530}))*((R_{760}/R_{700})-1)$	Gamon et al. (1992)	Leaf
Carotenoid/chlorophyll ratio index	PRI*CI	$(R_{680}-R_{500})/R_{750}$	Garrity et al. (2011)	Leaf
Plant senescencing reflectance Index	PSRI	$R_{672}/(R_{550}*3R_{708})$	Merzlyak et al. (1999)	Leaf
Reflectance band ratio index	Datt-CabCx + c	$R_{860}/(R_{550}*R_{708})$	Datt (1998)	Leaf
Reflectance band ratio index	DattNIRCabCx + c		Datt (1998)	Leaf

performed a sensitivity analysis of two spectral vegetation indices, the Normalized Difference Vegetation Index (NDVI) and the Angular Vegetation Index (AVI). Despite the efforts made to analyze $Cx+c$-related vegetation indices, further research should focus on understanding structural effects on $Cx+c$-related vegetation indices at canopy level.

The aim of the present study was to assess the estimation of carotenoid content in a complex conifer forest using high spatial and spectral resolution imagery and 3D canopy modeling methods. A combined observation and modeling approach was applied to assess the influence of leaf and canopy parameters on various narrow-band vegetation indices proposed to estimate carotenoid content. The specific objectives of the analysis were the following: i) assess the influence of carotenoid and chlorophyll content on the indices proposed, ii) evaluate the performance of existing narrow-band carotenoid indices at both leaf and canopy scales, iii) evaluate the sensitivity of $Cx+c$-related vegetation indices to canopy structure, and iv) propose a new formulation for $Cx+c$ estimation at canopy level, assessing its performance with high-resolution airborne imagery.

2. Materials and methods

2.1. Study site description

The experimental area was located in the Sierra de los Filabres mountain range (Almeria province, southeastern Spain) (37° 13′ 27″ N, 2° 32′ 54″ W) (Fig. 1), the driest region in Western Europe. The study area has an elevation ranging from 1540 to 2000 m above sea level and an annual rainfall between 300 and 400 mm. The annual average temperature is 11 °C, reaching a maximum of 32 °C in summer and a minimum of −8 °C in winter. The vegetation is a 40-year-old mixed pine afforestation of *Pinus sylvestris* L. Within the forest stands, the ground is partially covered by sparse evergreen shrub vegetation (*Adenocarpus decorticans* Boiss. and *Cistus laurifolius* L.). Parent material is composed of siliceous rock with quartz micaschists, forming eutric cambisol–regosol soils.

The study areas were located in seven different plots (Fig. 1). Leaf measurements were obtained from two consecutive field campaigns in July 2008 and August 2009. In 2008, needles were collected from a total of 21 trees, measuring $Ca+b$, $Cx+c$, the xanthophyll cycle (*VAZ*) pigment content and leaf reflectance. For 2009, needles collected from 35 trees were measured, analyzing pigment content ($Ca+b$, $Cx+c$).

2.2. Leaf measurements

Mean crown pigment and spectral measurements were obtained from a total of 5 young needles (one year-old needles) collected from the top of the crown. Analyses were performed on young needles to avoid non-representative outliers in current and mature needles. Needle pigment concentration was determined as reported by Abadía and Abadía (1993). Pigment extracts were obtained from a mixed sample of 5 cm of needle material, using 1 linear cm per needle. The area was calculated by assuming that the needle was a half cylinder and the diameter was the measured width of each needle. Needle diameter was measured with a digital caliper precision instrument. Five additional needle samples were used to take structural measurements (thickness and width) and determine water content and dry mass. The needles were ground in a mortar on ice with liquid nitrogen and diluted in acetone up to 5 ml (in the presence of Na ascorbate). After that, the extracts were filtered through a 0.45 μm filter to separate the pigment extracts from the Na ascorbate. Spectrophotometric and High-Performance Liquid Chromatography (HPLC) determinations were conducted simultaneously on the same extracts. A total of 20 μl was injected into the HPLC, and 1 ml was inserted into the spectrophotometer. The pigment extractions and HPLC measurements were undertaken concurrently to avoid pigment degradation. Absorption at 470, 644.8 and 661.6 nm was measured with the spectrophotometer to derive chlorophylls *a* and *b* and total carotenoid concentrations (Abadía & Abadía, 1993). Total chlorophyll and carotenoid concentration were related linearly with a mean coefficient of determination value of 0.59 per plot. Pigment extracts were analyzed using an isocratic HPLC method (Larbi et al., 2004). Samples were injected into a 100×8 mm Waters Novapak C18 radial compression column (4 μm particle size) with a 20 μl loop, and mobile phases were pumped by a Waters M45 high pressure pump at a flow of 1.7 ml/min. The EPS ratio between the pigment concentration was calculated as (V+0.5A)/(V+A+Z) (Thayer & Björkman, 1990), where V is violaxanthin, A is antheraxanthin and Z is zeaxanthin.

Needle spectral reflectance at wavelenghts from 306 to 1138 nm was also measured with a UniSpec Spectral Analysis System (PP Systems, Herts, UK), following a similar procedure to that described by Richardson and Berlyn (2002). The UniSpec measurements were conducted in the field minutes before the needles were collected. The instrument has a resolution of <10 nm and 256 bands spaced at 3.3 nm intervals. The instrument was configured using a mini bifurcated fiberoptic and a mini leaf clip capable of measured spectral reflectance on tiny samples (<1 mm). A Spectralon reflectance standard was regularly referenced and scans were corrected for the instrument's dark current. The reflectance spectrum for each scan was calculated as a ratio of leaf radiance to standard radiance at wavelength λ. Six separate measurements were made in a 1-cm diameter area and average of those spectra was used for subsequent analyses. Needle reflectance obtained from the field was used to evaluate the relationships between hyperspectral indices and pigment content at the leaf level.

2.3. Airborne campaigns

An unmanned aerial vehicle (UAV) platform for remote sensing research was developed at the Laboratory for Research Methods in Quantitative Remote Sensing (QuantaLab, IAS-CSIC, Spain) to carry a payload with narrow-band multispectral imaging sensors (Berni et al., 2009; Zarco-Tejada et al., 2009). The UAV was a 2-m fixed-wing platform capable of carrying a 3.5 kg payload. It had 1 hour endurance and 5.8 kg take-off weight (TOW) (mX-SIGHT, UAV Services and Systems, Germany). The UAV was controlled by an autopilot for autonomous flight (AP04, UAV Navigation, Madrid, Spain) to follow a flight plan using waypoints. The autopilot consisted of a dual CPU that controlled an integrated Attitude Heading Reference System (AHRS) based on a L1 GPS board, 3-axis accelerometers, yaw rate gyros and a 3-axis magnetometer (Berni et al., 2009). Communication with the ground was conducted through a radio link where position, attitude and status data were transmitted at 20 Hz frequency; this also acted as a communication link for operating remote sensing multispectral cameras on board the UAV.

The multispectral sensor used in this study was a 6-band multispectral camera (MCA-6, Tetracam, Inc., California, USA). The camera consisted of 6 independent image sensors and optics with user-configurable spectral filters. The image had a resolution of 1280×1024 pixels with 10-bit radiometric resolution and an optical focal length of 8.5 mm, yielding an angular FOV of 42.8°×34.7° and

Table 2
Nominal values range of parameters used for leaf modeling with *PROSPECT-5*.

Prospect-5 input variables	Value	Unit
$Ca+b$ (varied parameter)	10–60	μ g cm^{-2}
$Cx+c$ (varied parameter)	2–16	μ g cm^{-2}
Cw	0.03	cm
Cm	0.01	g cm^{-2}
N	2	

15 cm pixel spatial resolution at 150 m flight altitude. The detector used was a CMOS sensor with ~5.2 μm pixel size and 6.66 mm × 5.32 mm image area operated in a progressive scan mode at 54 dB signal-to-noise ratio, with 0.03% fixed pattern noise, 28 mV/s dark current and 60 dB dynamic range. Different bandsets were selected depending on the objectives of the remote sensing study, including 25 mm diameter bandpass filters of 10 nm FWHM (Andover Corporation, NH, USA), with center wavelengths at 515 nm, 530 nm, 570 nm,

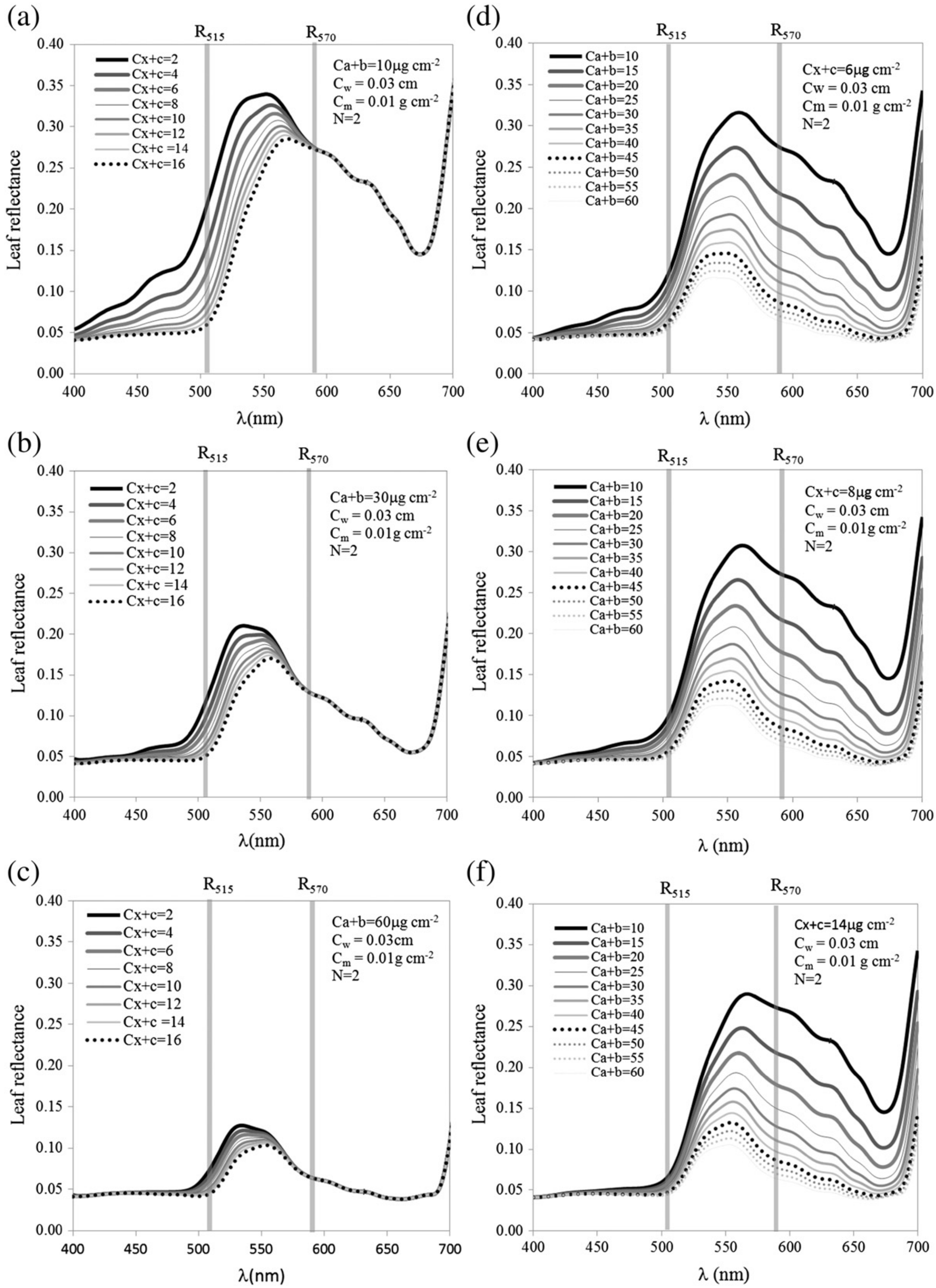

Fig. 2. Leaf-level modeling simulations conducted with the PROSPECT-5 model to assess the effects of *Cx + c* and *Ca + b* contents on the spectral signature in the 400–700 nm spectral range. Simulations performed for *Cx + c* variation between 2 and 16 μg cm^{-2} for mean *Ca + b* values of 10, 30 and 60 μg cm^{-2} (a,b,c). Simulations conducted for *Ca + b* variation between 10 and 60 μg cm^{-2} for mean *Cx + c* values of 6, 8 and 14 μg cm^{-2} (d,e,f).

670 nm, 700 nm, and 800 nm bands. The 10 nm filter measurements yielded ca. 60% transmission and 10.4 nm FWHM.

Multispectral imagery was radiometrically calibrated using coefficients derived from measurements taken with a calibrated uniform light source (integrating sphere, CSTM-USS-2000C Uniform Source System, LabSphere, NH, USA) at four different levels of illumination and six different integration times. Radiance values were later converted to reflectance using the total incoming irradiance simulated with the SMARTS model developed by the National Renewable Energy Laboratory of the US Department of Energy (Gueymard, 1995, 2001) using aerosol optical depth measured with a Micro-Tops II sun photometer (Solar LIGHT Co., Philadelphia, PA, USA) collected in the study areas at the time of the flights. SMARTS computes clear-sky spectral irradiance, including direct beam, circumsolar, hemispherical diffuse and total irradiance on a tilted or horizontal plane in specific atmospheric conditions. This radiative transfer model has previously been used in other studies to perform the atmospheric correction of narrow-band multispectral imagery (Suárez et al., 2010; Zarco-Tejada et al., 2012). The calibrated multispectral reflectance imagery obtained at 10 nm FWHM is shown in Fig. 1b, targeting pure components such as crowns, shaded and sunlit soil spectra (Fig. 1b). Each individual pure tree crown in the entire forest canopy was identified using automatic object-based crown-detection algorithms (Ardila et al., 2012; Kurtz et al., 2012) based on the Normalized Difference Vegetation Index (NDVI) calculated from the high spatial resolution image using the 670 and 800 nm spectral bands. This made it possible to extract the mean crown reflectance.

Field sampling campaigns were conducted concurrently with UAV overflights in the last week of August 2009. The flight campaigns were performed at 10 a.m. (GMT). A total of 35 individuals of *P. sylvestris* were subjected to field and airborne monitoring (Fig. 1). The measurements were taken on trees of a similar age (~40 years old) and height (~10 m) growing in low slope areas (<10%) and therefore with a similar sun/shade fraction.

2.4. Optical indices for $Cx+c$ estimation

The purpose of this analysis was to evaluate the performance of a set of hyperspectral vegetation indices in carotenoid content estimation. The performance of each vegetation index was evaluated based on simulation analysis and field measurements. Vegetation indices calculated from simulation analysis at the leaf level were compared to the results obtained from field measurements. At the canopy level, vegetation indices calculated from reflectance simulations were compared to results obtained from the image reflectance acquired with a narrow-band multispectral camera. A detailed summary of the narrow-band vegetation indices applied in this study is shown in Table 1. The narrow-band vegetation indices selected from previous studies for $Cx+c$ estimation were combinations of bands located in the visible and visible/NIR region. In previous studies, PRI was calculated with the 570 nm band as a reference (PRI_{570}) and later with the 515 nm band as a reference (PRI_{515}) and has been found to minimize structural effects (Hernández-Clemente et al., 2011). Similar wavelengths have been selected by Gitelson et al. (2003, 2006) to formulate the Carotenoid Content Index (CRI_{550}). Other indices have been formulated as a combination of bands around $R_{510-515}$ and $R_{700-770}$. A few examples are CRI_{700}, $RNIR^{*}CRI_{550}$ and $RNIR^{*}CRI_{700}$, proposed by Gitelson et al. (2003, 2006); the Ratio Analysis of Reflectance Spectra, proposed by Chappelle et al. (1992) as RARS; the Carotenoid/Chlorophyll Ratio Index (PRI*CI), analyzed by Garrity et al. (2011); the Reflectance Band Ratio Index (RBRI), proposed by Datt (1998) and the Plant Senescence Reflectance Index (PSRI), proposed by Merzlyak et al. (1999). The last group of $Cx+c$-related optical indices previously published is combinations of visible bands with the bands R_{800} or R_{860}. Some examples are the Pigment-Specific Simple Ratio (PSSRa, PSSRb, PSSRc, PSNDc), analyzed by Blackburn (1998), and the $RBRI_{NIR}$, analyzed by Datt (1998).

New narrow-band ratio indices in the 500–600 nm regions were also assessed at both leaf and crown levels for sensitivity to $Cx+c$. Narrow-band ratio indices were formulated based on relationships to the absorption of $Cx+c$ concentration (the blue region from 450 to 555 nm) divided by the immediately contiguous bands located in the green region (560 and 570 nm reference bands).

2.5. Simulations with PROSPECT-5 and DART models

A model simulation analysis was conducted to assess the sensitivity of the carotenoid-related optical indices on heterogeneous coniferous forest canopy images and to test the performance of new formulations. Radiative transfer modeling methods were applied with the leaf optical PROperties SPECTra (PROSPECT-5) model (Féret et al., 2008; Jacquemoud & Baret, 1990) coupled with the 3-dimensional Discrete Anisotropic Radiative Transfer (DART) model.

PROSPECT-5 was selected for the leaf-level simulations. This model simulates leaf directional–hemispherical reflectance and transmittance from the 400 to the 2500 nm spectral region with five input variables: $Ca+b$, $Cx+c$, leaf dry matter content (Cm), equivalent water thickness (Cw) and leaf structure parameter (N) (Féret et al., 2008). Although the PROSPECT model was originally developed for broad leaves, it has been validated and is widely used for needles (Malenovsky et al., 2007; Moorthy et al., 2008; Zarco-Tejada et al., 2004). Leaf-level simulations with PROSPECT-5 were performed to assess the effect of $Cx+c$ and $Ca+b$ content variations on the spectral signature in the 400–800 nm region and on the optical indices proposed, both at leaf and canopy levels when coupled with the DART model. Nominal values and input parameter ranges used for the leaf modeling are summarized in Table 2. Fixed values for Cw, Cm and N and the variation range for $Cx+c$ and $Ca+b$ were set based on previous studies carried out on conifer species (Hernández-Clemente et al., 2011; Moorthy et al., 2008). Fig. 2 shows an example of the spectral variation derived from the simulations performed had a range of 2–16 μg cm^{-2} for $Cx+c$ and a mean $Ca+b$ value of 10, 30 and 50 μg cm^{-2} (Fig. 2a, b, c). Additional simulations showed $Ca+b$ variation, ranging from 10 to 60 μg cm^{-2} along with $Cx+c$ values of 6, 8 and 14 μg cm^{-2} (Fig. 2d, e, f).

At crown level, DART was chosen because it simulates the radiative transfer in complex structures. This model was used in this

Table 3
Nominal values range of parameters used for canopy modeling with *DART*.

DART input variables	Value	Unit
Central wavelength	400–800	nm
Spectral bandwidth	10	nm
Scene parameters		
Cell size	0.5	m
Scene dimensions	50×50	m
Spatial distribution	Random	
Canopy parameters		
Number of trees	1200 trees ha^{-1}	
Probability of presence	0.8	
Leaf area index (varied parameter)	1–10	
Crown shape	Truncated cone	
Crown height (mean)	6	m
Crown height (std dev)	0.9	m
Height below crown (mean)	4	m
Height below crown (std dev)	0.8	m
Diameter below crown (mean)	0.4	m
Diameter below crown (std dev)	0.1	m
Height within the tree crown	5	m
Diameter within the tree crown	0.35	m

study to generate coniferous canopy architectures at high spatial resolution. DART was developed by Gastellu-Etchegorry et al. (1996) on the basis of the discrete ordinate method (DOM). DART has been used to simulate heterogeneous coniferous forest canopies (Malenovsky et al., 2008) and has been validated for this use (Pinty et al., 2001; Widlowski et al., 2007). In order to simulate the forest canopy architecture of the study sites, the DART model was parameterized based on detailed field measurements.

The coupled PROSPECT and DART models were used to simulate the spectral reflectance of *P. sylvestris* forest stands assuming random variations of $Ca+b$ and $Cx+c$ content under two different scenarios: i) considering a random variation in LAI (Leaf Area Index) (1–10); ii) considering variations in both LAI (1–10) and tree density (800–1600 trees ha^{-1}). In both cases, PROSPECT simulations were based on random $Cx+c$ (2–16 µg cm^{-2}) and $Ca+b$ (10–60 µg cm^{-2}) values. Nominal values and the parameter range used for crown modeling are summarized in Table 3. Canopy level simulations were performed using the hemispherical reflectance simulated at the leaf level with PROSPECT. An example of the canopy reflectance simulated with PROSPECT coupled with DART is shown in Fig. 3. Fig. 4 shows the crown reflectance of trees with low (LAI = 1) and high (LAI = 5) LAI values simulated with DART based on leaf reflectance and

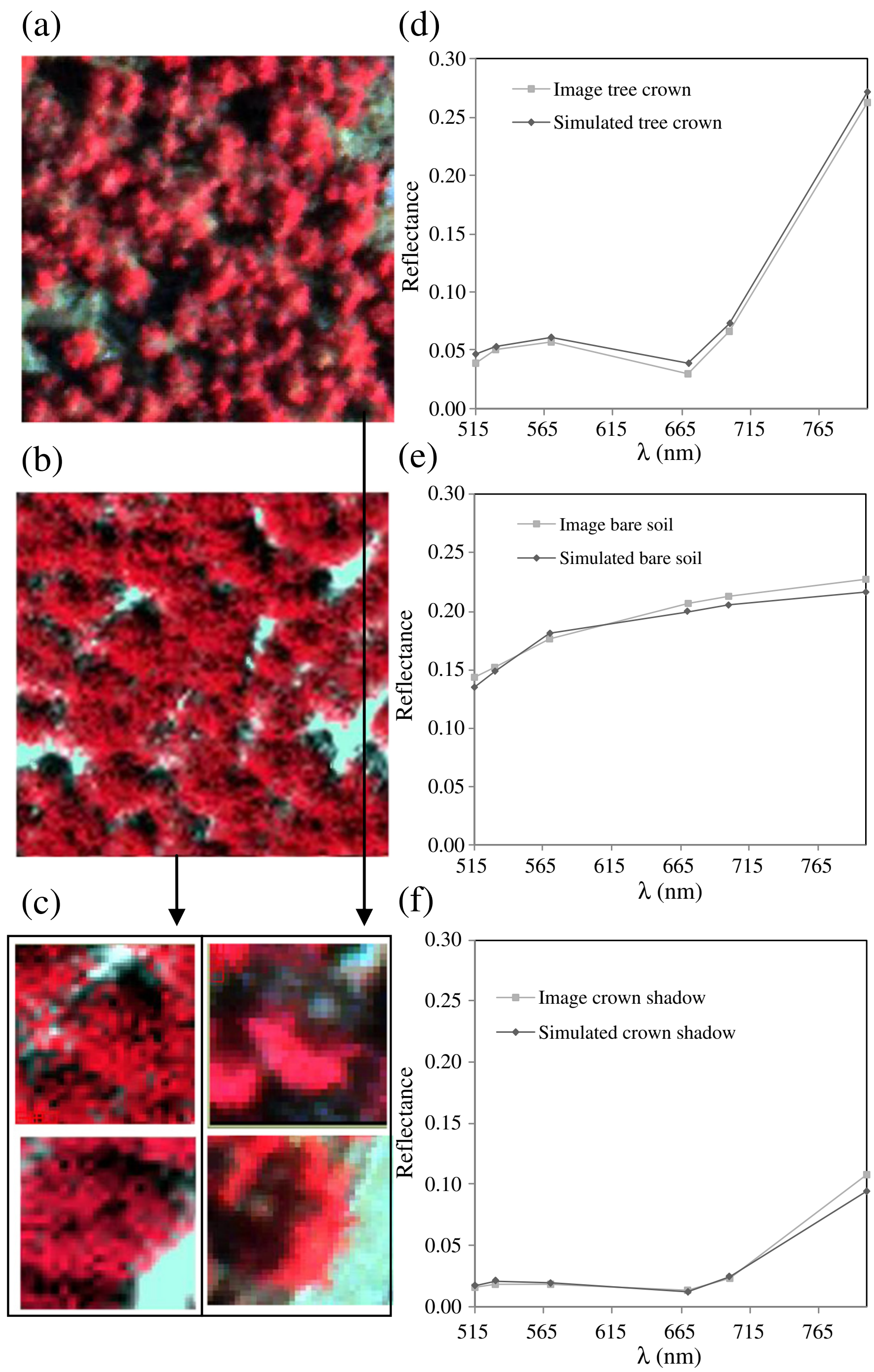

Fig. 3. High-resolution multispectral image acquired from the UAV platform (a) and the PROSPECT-5 + DART simulated image for the same study site (b); zoomed-in image detail of the multispectral image (right) and the simulated image (left) (c); tree crown (d), bare soil (e) and shaded crown (f) spectral reflectance extracted from the multispectral image and the simulated scenes.

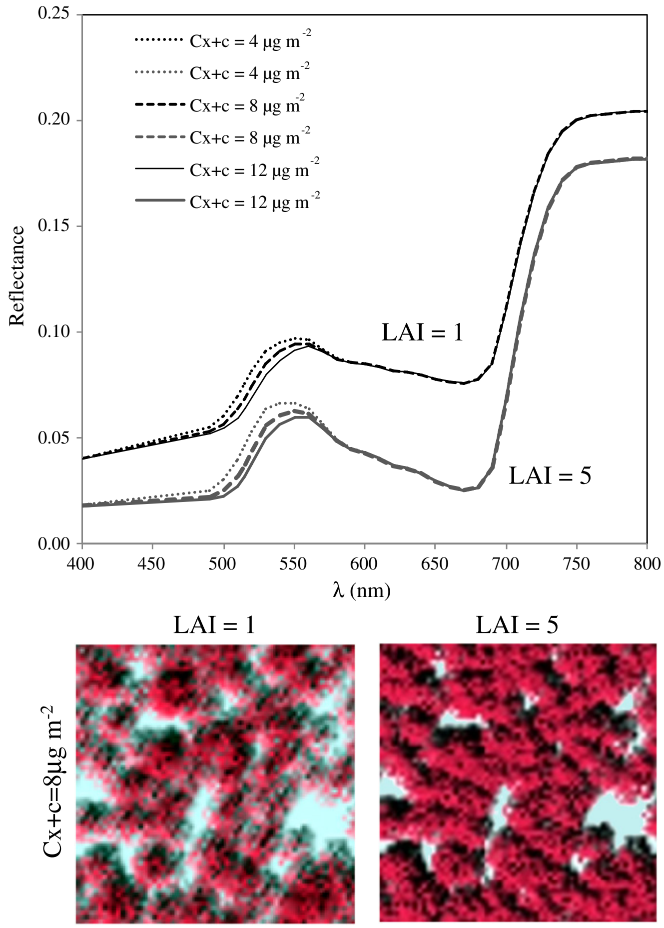

Fig. 4. Canopy reflectance simulated with PROSPECT-5 + DART models considering low LAI (LAI = 1) and high LAI values (LAI = 5) for different concentrations of *Cx* + *c* (4, 8 and 12 μg cm^{-2}) and a mean *Ca* + *b* value of 35 μg cm^{-2}.

transmittance. Leaf reflectance and transmittance were simulated with PROSPECT-5 considering different values of carotenoid content (4, 8 and 12 μg m^{-2}) and a mean value of chlorophyll content (35 μg m^{-2}).

3. Results

3.1. Leaf-level simulation results

Simulations conducted with the PROSPECT-5 model assessed the sensitivity of the various vegetation indices to different values of *Ca* + *b* and *Cx* + *c* content. The simulations showed that chlorophylls *a* and *b* have strong absorbance peaks in the blue and red regions of the spectrum (from 500 to 700 nm) (Fig. 2d, e, f). Carotenoid absorbance mainly affected the 450 to 555 nm region (Fig. 2a, b, c), overlapping chlorophyll absorption peaks from 500 to 555 nm. The vegetation indices proposed were formulated as a simple ratio between bands located in the carotenoid and chlorophyll absorbance spectral range (Fig. 2).

Coefficients of determination (r^2) of all the indices studied are provided in Fig. 5, which shows the relationships found between simulated hyperspectral vegetation indices and pigment content. Most of the *Cx* + *c*-related vegetation indices tested at leaf level showed good agreement with *Cx* + *c* content. The best relationships were obtained when the CRI_{550} and CRI_{700} indices were used. The linear relationship between such CRI indices and *Cx* + *c* was significant (P<0.001), with a coefficient of determination of r^2>0.9. By contrast, the relationship between these CRI indices and *Ca* + *b* had a coefficient of determination of less than 0.15. These results showed the sensitivity of CRI indices to *Cx* + *c* content and their low sensitivity to chlorophyll content at leaf level. Other indices such as $RNIR \cdot CRI_{550}$ and $RNIR \cdot CRI_{700}$ were found to be highly correlated with *Cx* + *c*, with a coefficient of determination of r^2 = 0.72 and r^2 = 0.74 respectively, but were more influenced by *Ca* + *b* (r^2>0.3) (Fig. 5). In the leaf-level simulations a 1% Gaussian random noise was added to the leaf simulations (Fig. 5). This step aimed at assessing noise-sensitive indices as shown in le Maire et al. (2004). According to the results obtained with and without the Gaussian noise (Fig. 5), the simulated spectral vegetation indices showed similar sensitivity to *Ca* + *b*, *Cx* + *c* and to the *Ca* + *b*/*Cx* + *c* ratio.

The comparative analysis performed by testing a large number of *Cx* + *c* indices identified a new group of indices that were significantly related to *Cx* + *c* (P<0.001) but showed low sensitivity to *Ca* + *b* content (r^2<0.15). This was the case of PRI_{m1}, with a coefficient of determination of r^2 = 0.86 and the following ratio indices: R_{515}/R_{560} (r^2 = 0.80), R_{520}/R_{560} (r^2 = 0.79), R_{510}/R_{560} (r^2 = 0.77), R_{515}/R_{570} (r^2 = 0.71), R_{510}/R_{570} (r^2 = 0.69), R_{520}/R_{570} (r^2 = 0.68) and R_{530}/R_{570} (r^2 = 0.54).

The relationship between the indices SR_{560} (R_{510}, R_{515}, R_{520} and R_{530} over R_{560}) and SR_{570} (R_{510}, R_{515}, R_{520} and R_{530} over R_{570}) and *Cx* + *c* is presented in Fig. 6, which shows the behavior of the new ratio indices proposed in this study. These indices showed similar trends and coefficients of determination to *Cx* + *c* content, with the best relationships observed for R_{515}/R_{570} (r^2 = 0.72) (Fig. 6a) and R_{515}/R_{560} (r^2 = 0.80) (Fig. 6b). Other *Cx* + *c*-related vegetation indices showed significant relationships (P<0.001) with *Cx* + *c* content (r^2>0.5), but were more affected by chlorophyll content (r^2>0.3). This was the case of the indices PRI and RARS, as well as the simple ratios R_{500}/R_{560}, R_{530}/R_{570}, and R_{540}/R_{560}.

In the case of *Ca* + *b*, the best relationships were obtained using the vegetation indices CIred edge and PSSRb, yielding a coefficient of determination higher than 0.98 (Fig. 5). Despite using other indices such us PSSRa, DattNIR-CabCar or TCARI/OSAVI, relationships from r^2 = 0.8 to r^2 = 0.9 were found. In addition, the *Cx* + *c*/*Ca* + *b* ratio was found to be a variable highly related with a wide range of vegetation indices due to the sensitivity of such indices either to *Cx* + *c* or *Ca* + *b* concentration (Fig. 5). The best relationship with *Cx* + *c*/*Ca* + *b* was found for indices such as PSRI and PRI, yielding a coefficient of determination around 0.9.

3.2. Canopy-level simulation results

Simulations conducted with DART at canopy level were used to assess the effect of the structure on the *Cx* + *c* indices when targeting pure crowns. Results of the modeling analysis showed that vegetation indices behaved differently at leaf and crown level (Fig. 7). These results show that the closest relationships between *Cx* + *c* content and vegetation indices at crown level were obtained by the indices R_{515}/R_{570} and R_{520}/R_{570}, yielding r^2 values of 0.70 and 0.71 respectively. Simple ratios formulated with bands from R_{510} to R_{540} and the reference bands R_{560} and R_{570} showed significant relationships (P<0.001) and coefficients of determination greater than 0.55 (Fig. 7). Other vegetation indices highly correlated with *Cx* + *c* content at leaf level showed high effects due to the structure and did not obtain high coefficients of determination at crown level. This was the case of CRI_{550} (r^2 = 0.44) and CRI_{700} (r^2 = 0.43). These results are in agreement with studies that have shown that leaf-level indices may not work well at canopy level due to the confounding effects of the structure on the indices. The vegetation indices proposed by Gitelson were formulated based on spectral bands simulated with 10 and 30 nm FWHM. This analysis was conducted to assess the effect of considering different band widths for the 510–520 nm and 540–560 nm ranges. The results shown in Fig. 8 demonstrate that comparable results were obtained for (10 and 30 nm FWHM).

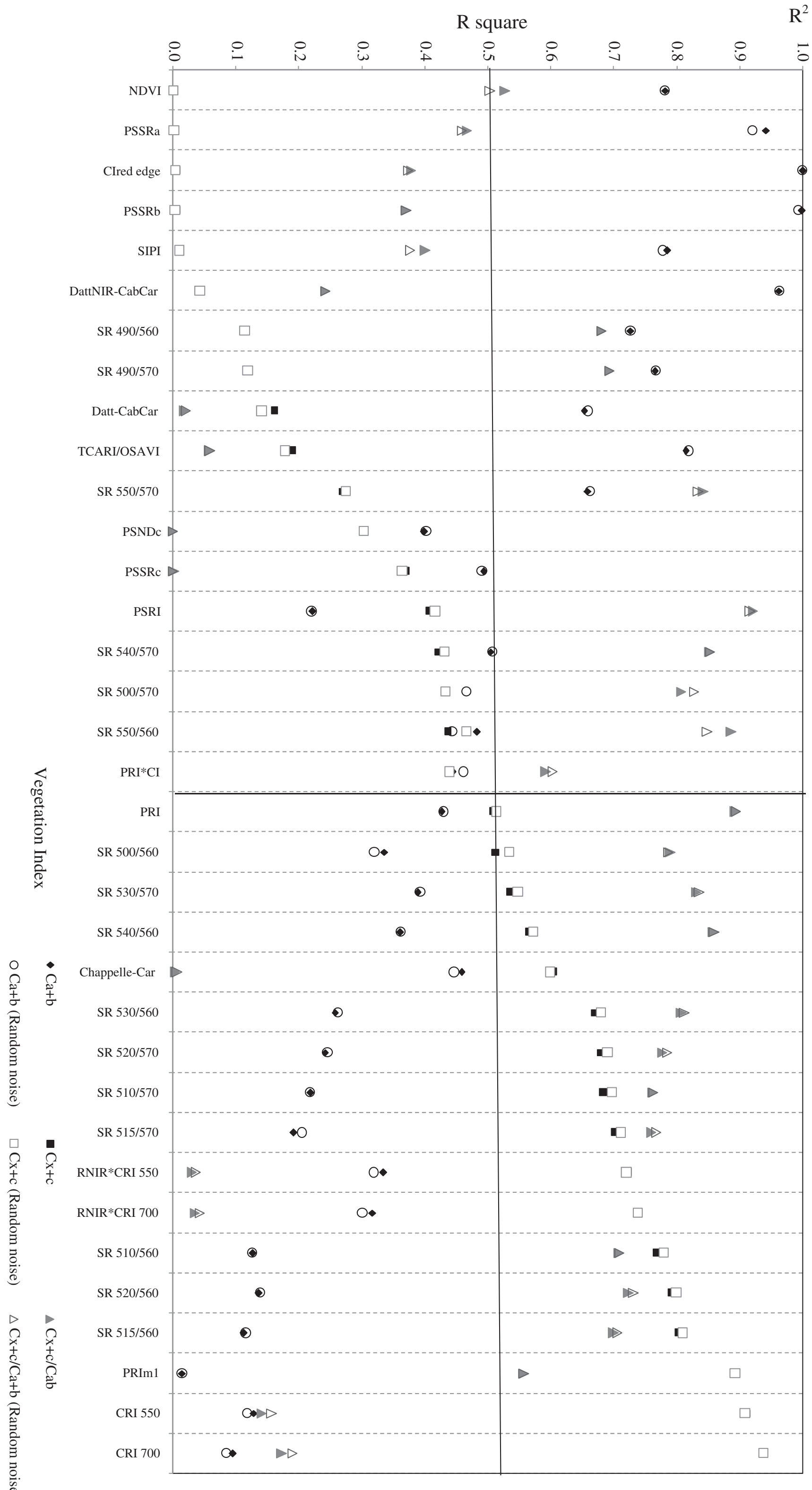

Fig. 5. Relationships obtained between *Ca* + *b*, *Cx* + *c* content and the *Ca* + *b*/*Cx* + *c* ratio when compared with vegetation indices proposed for *Cx* + *c* estimation. Data were simulated at leaf level with PROSPECT-5 model assuming random *Cx* + *c* (2–16 μg cm^{-2}) and *Ca* + *b* content (10–60 μg cm^{-2}). When symbols overlap, the *r* square calculated considering random noise has precedence.

A comparison of the relationships found in a selection of indices at both leaf and crown levels is provided in Fig. 9. While R_{515}/R_{570} showed similar agreement with *Cx* + *c* at leaf and crown levels ($r^2 = 0.7$) (Fig. 9a and c), other indices such as CRI_{550} and CRI_{700} showed a high coefficient of determination at leaf level ($r^2 = 0.9$) (Fig. 9b) but poorer performance at crown level ($r^2 = 0.44$) (Fig. 9d). These results demonstrate the importance of accounting for canopy-level effects on the indices and assessing the performance

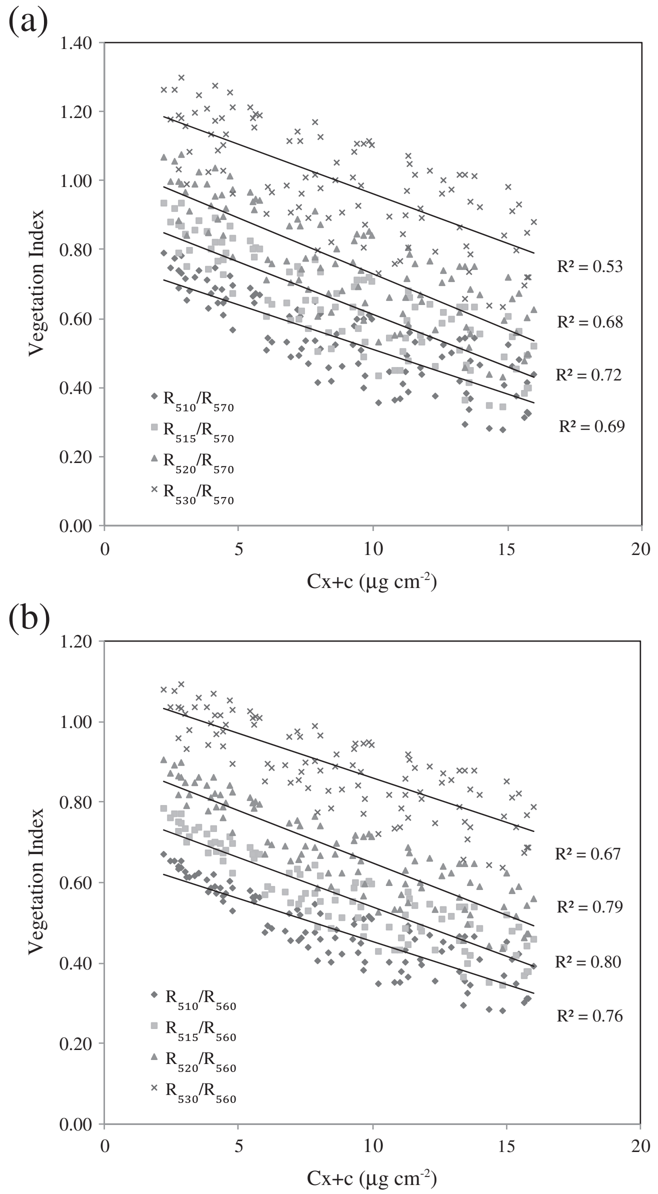

Fig. 6. Relationships obtained between *Cx* + *c* content and the simple ratio vegetation indices $R_{510/570}$, $R_{515/570}$, $R_{520/570}$, and $R_{530/570}$ (a) and $R_{510/560}$, $R_{515/560}$, $R_{520/560}$, and $R_{530/560}$ (b). Simulations conducted at leaf level with the PROSPECT-5 model considering random *Cx* + *c* (2–16 µg cm^{-2}) and *Ca* + *b* content (10–60 µg cm^{-2}).

at both leaf and canopy levels. These results can be explained by the different sensitivities of these indices to structural effects. As shown in Fig. 10, the coefficients of determination between the vegetation indices CRI_{550} and CRI_{700} and LAI values were $r^2 = 0.48$ and $r^2 = 0.45$ respectively (Fig. 10a and b). By contrast, the relationship between simple ratio indices such as R_{515}/R_{570} and R_{540}/R_{560} and LAI showed coefficients of determination of less than 0.05 (Fig. 10c and d). These simulation results demonstrate the low effects of LAI variation on the *Cx* + *c* index proposed in this study (R_{515}/R_{570}), with coefficients of determination of $r^2 = 0.72$ for *Cx* + *c* and $r^2 = 0.19$ for *Ca* + *b* at leaf level and $r^2 = 0.71$ for *Cx* + *c* and $r^2 = 0.16$ for *Ca* + *b* at canopy level.

A more detailed analysis of the structural variation affecting *Cx* + *c*-related indices was performed normalizing the values of vegetation indices to LAI = 1. Fig. 11 shows the variations of CRI_{550} (Fig. 11a), RARS (Fig. 11b), R_{515}/R_{570} (Fig. 11c) and R_{540}/R_{560} (Fig. 11d), considering a range for LAI (1–10) and tree density (800–2800 trees ha^{-1}). While some vegetation indices such as R_{515}/R_{570} and R_{540}/R_{560} were not affected, the RARS and CRI_{550} indices showed higher sensitivity to LAI and tree density variation.

LAI variations also seem to affect the relationships between *Cx* + *c*-related vegetation indices and the *Cx* + *c*/*Ca* + *b* ratio. Indices with high coefficient of determination values ($r^2 = 0.9$) at leaf level such as PSRI or PRI yielded coefficients of determination of $r^2 = 0.46$ and $r^2 = 0.64$ at crown level (Fig. 7).

3.3. Relationships between optical indices and Cx + c obtained from leaf measurements and airborne imagery

The analysis of the leaf measurements showed significant relationships between *Cx* + *c* indices and needle *Cx* + *c* content obtained by destructive sampling. The coefficients of determination calculated by the linear regression analysis are shown in Fig. 12. The experimental results agree with the results obtained with model simulations, in which indices such as CRI_{700} ($r^2 = 0.73$) or CRI_{550} ($r^2 = 0.72$) (Fig. 12a and c) showed better results than the R_{515}/R_{570} index ($r^2 = 0.57$) at leaf level (Fig. 12b). A further comparison between the R_{515}/R_{570} vegetation index and the epoxidation state (EPS) of the xanthophyll cycle yielded a coefficient of determination of $r^2 = 0.12$ (Fig. 12d). These results demonstrate that SR (R_{515}/R_{570}) was correlated with *Cx* + *c* content but was not sensitive to variations in the xanthophyll cycle. The R_{515}/R_{570} index showed a weak relationship with *Ca* + *b* content, with a coefficient of determination of $r^2 = 0.10$ (Fig. 13a). This result agrees with the modeling results obtained with PROSPECT-5, where the relationship between R_{515}/R_{570} and *Ca* + *b* was lower than 0.15. As expected, the strongest relationships were found between *Ca* + *b* content and the red edge index R_{750}/R_{710} (Fig. 13b).

The high spatial resolution imagery (50 cm) obtained with the narrow-band multispectral camera enabled the identification of pure crowns and the assessment of pigment measurements by applying vegetation indices to the crown level. Linear relationships obtained between *Cx* + *c* content and the simple ratio index R_{515}/R_{570} showed a significant relationship ($p < 0.001$), with a coefficient of determination of $r^2 = 0.66$ (Fig 14a). Other traditional indices sensitive to *Cx* + *c* content at leaf level (CRI) showed weaker relationships at crown level (Fig 14c). These results agree with the results of coupling PROSPECT-5 with DART simulations, where the R_{515}/R_{570} index behaved better than the CRI indices at crown level. The relationships obtained between the simple ratio index R_{515}/R_{570} and *Ca* + *b* content showed a low coefficient of determination ($r^2 = 0.18$) (Fig. 14b). By contrast, *Ca* + *b*-related vegetation indices were found to be highly related with *Ca* + *b* content ($r^2 = 0.71$) (Fig. 14d). These results agree with the findings obtained at leaf level, where the simple ratio index R_{515}/R_{570} was highly related with *Cx* + *c* content and slightly related with *Ca* + *b*, while the *Ca* + *b*-related vegetation index R_{700}/R_{570} was highly related with *Ca* + *b* content.

The relationship found between *Cx* + *c* and R_{515}/R_{570} (Fig. 14a) was used to map carotene spatial variability at crown level using high-resolution imagery. Fig. 15 shows a map of the *Cx* + *c* content of the study area aggregated into different classes, where values correspond to very low *Cx* + *c* content (<2 µg cm^{-2}), low *Cx* + *c* content (range 2–4 µg cm^{-2}), below average *Cx* + *c* content (range 4–6 µg cm^{-2}), average *Cx* + *c* content (range 6–8 µg cm^{-2}), average to above-average *Cx* + *c* content (range 8–10 µg cm^{-2}), above-average *Cx* + *c* content (range 10–12 µg cm^{-2}), high *Cx* + *c* content (range 12–14 µg cm^{-2}) and very high *Cx* + *c* content (range 14–16 µg cm^{-2}).

4. Discussion

The quantitative link between foliar carotenoid content and spectral properties constitutes the basis of pigment retrieval analysis. Several studies have been conducted at leaf scale (Chappelle et al., 1992; Gitelson et al., 2002; Merzlyak et al., 1999). The present study includes a comprehensive review of narrow-band vegetation indices

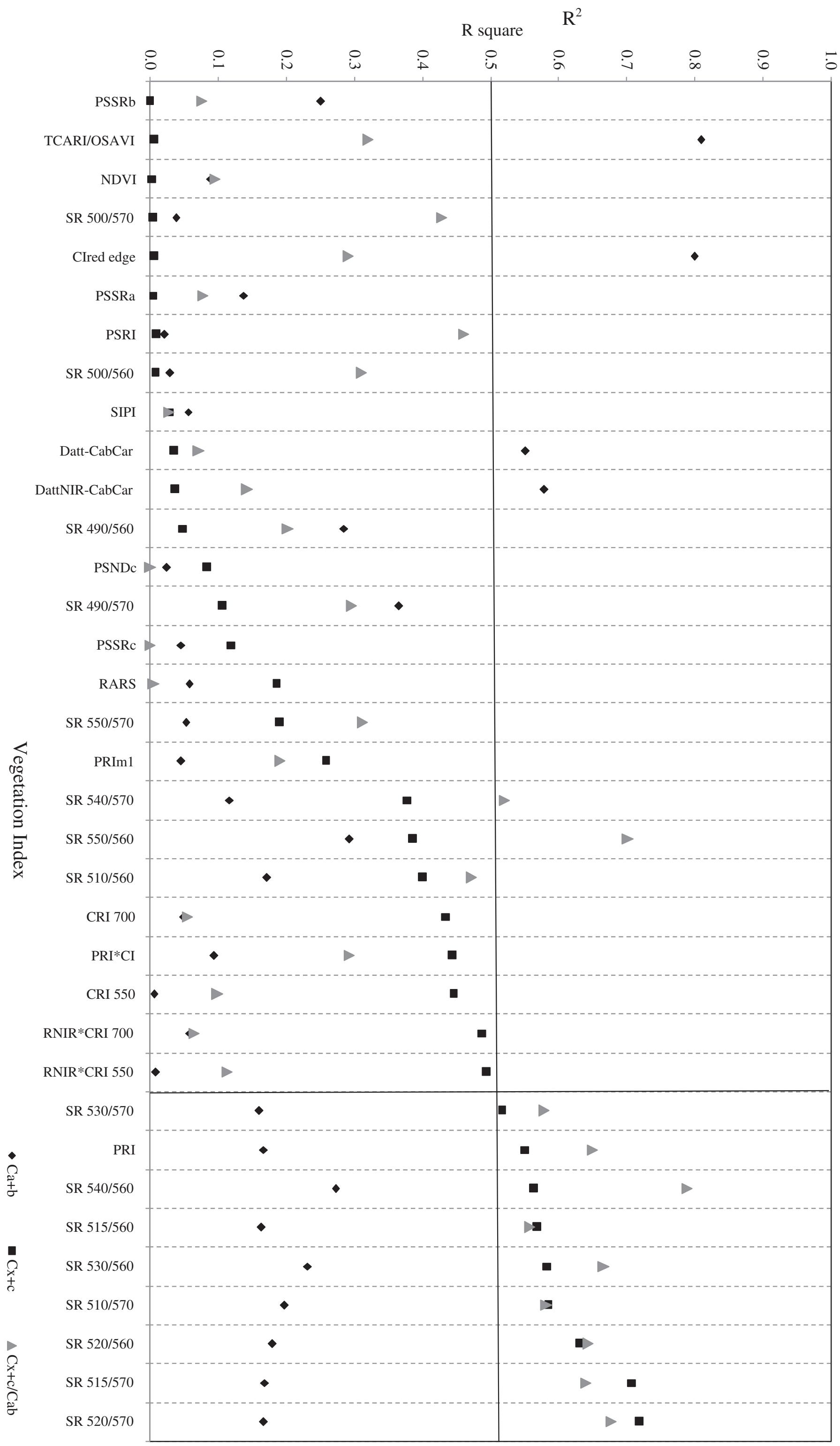

Fig. 7. Relationships obtained between $Ca+b$, $Cx+c$ content and the $Ca+b/Cx+c$ ratio when compared with vegetation indices proposed for $Cx+c$ estimation. Data were simulated at crown level with PROSPECT-5 model coupled with DART assuming random variation of leaf $Cx+c$ (2–16 μg cm^{-2}) and $Ca+b$ (10–60 μg cm^{-2}) and crown LAI ranging between 1 and 8.

related to carotenoid content based on empirical and modeling methods. Formulating $Cx+c$-related vegetation indices is more challenging than retrieving other biophysical parameters mainly due to the overlap between the chlorophyll and carotenoid absorption peaks. Red edge and TCARI/OSAVI vegetation indices obtained from the simulation analysis showed high sensitivity to $Ca+b$ at leaf and canopy levels. These results agree with previous studies that used red edge vegetation indices in forest canopies (Moorthy et al., 2008; Zarco-Tejada et al., 2001) and applied combined indices such as TCARI/OSAVI in tree orchards (Zarco-Tejada et al., 2004) and vineyards (Meggio et al., 2010). Simulation results performed at leaf level provide additional information about the sensitivity of these

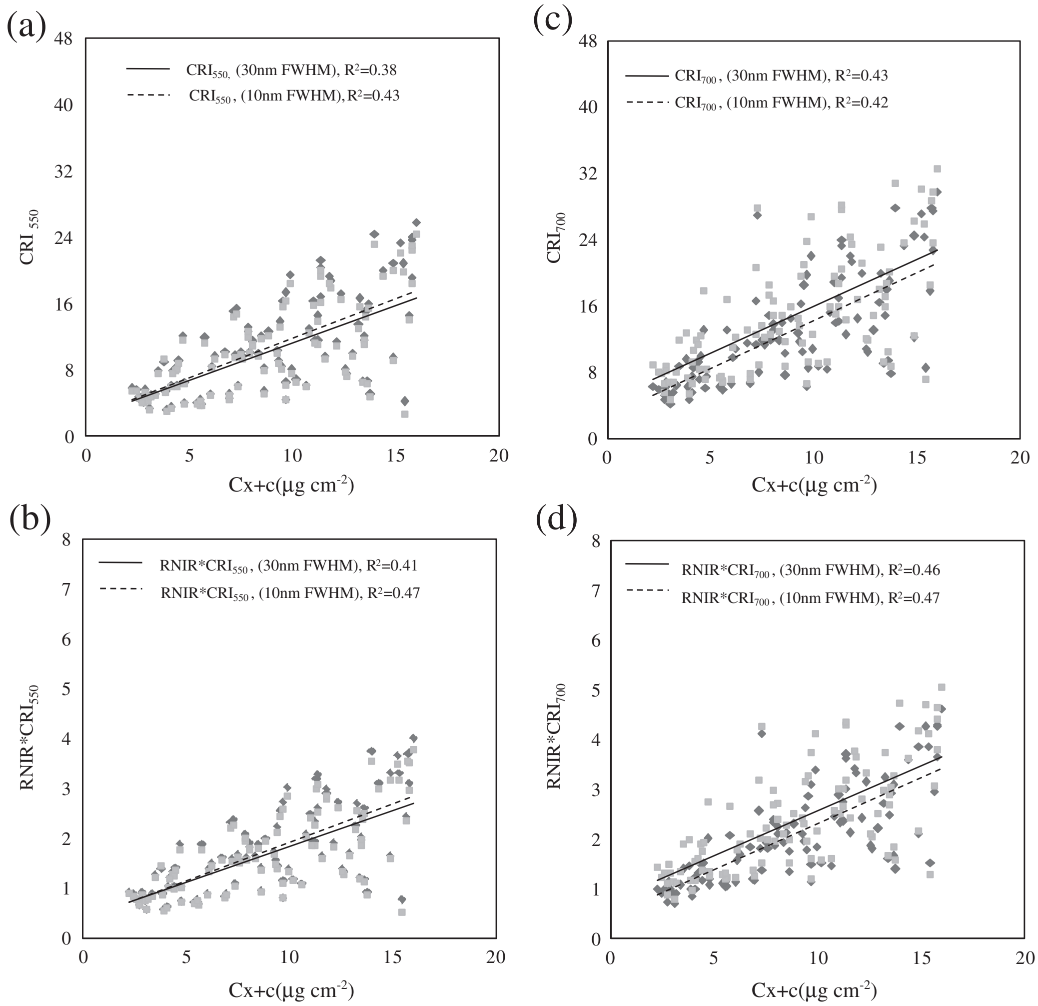

Fig. 8. Relationships obtained between $Cx+c$ and vegetation indices CRI_{550} (a), RNIR*CRI_{550} (b). CRI_{700} (c) and RNIR*CRI_{700} (d) formulated with 10 and 30 nm FWHM at crown level.

indices to $Ca+b$ concentration and the $Cx+c/Ca+b$ ratio. The interest of analyzing the relationships between those variables and the response of $Ca+b$ sensitivity to $Cx+c$-related vegetation indices has been previously studied for some of the indices included in this study such as the CRI (Gitelson et al., 2002) and the PRI (Garrity et al., 2011). The $Cx+c/Ca+b$ ratio was found to be highly related with a wide range of $Cx+c$-related vegetation indices at the leaf level, although the best relationship was found using the PSRI and PRI vegetation indices. These results agree with those obtained by Merzlyak et al. (1999) (PSRI) and Garrity et al. (2011) (PRI) at the leaf level. However, according to the results obtained at crown level, these indices seem to be highly affected by structural parameters.

A detailed sensitivity analysis of the effect of structural parameters such as LAI or tree density introduced into the Discrete Anisotropic Radiative Transfer (DART) model was performed to show the potential scaling-up of $Cx+c$-related vegetation indices in heterogeneous canopies. Coefficients of determination resulting from the linear relationships between $Cx+c$ content and narrow-band vegetation indices revealed the ability of simple ratio indices to assess variations in $Cx+c$ content, showing better results than traditional $Cx+c$-related vegetation indices at crown level. Traditional indices formulated as a combination of visible and infrared bands showed greater sensitivity to structural variable effects than simple ratio indices formulated as a combination of bands influenced by $Cx+c$ and $Ca+b$ absorption.

The new simple ratio vegetation indices proposed in this study were found to be significantly related with $Cx+c$ content ($r^2>0.6$; $P<0.001$) at leaf and crown levels. Nevertheless, this study confirms the robustness of other indices such as the CRI_{550} ($r^2>0.93$; $P<0.001$) and CRI_{700} ($r^2>0.91$; $P>0.001$) reported in previous studies at leaf level (Gitelson et al., 2003, 2006). Model simulations were validated with detailed laboratory/field leaf pigment content measurements ($Ca+b$, $Cx+c$ and xanthophyll pigment content) and needle spectral reflectance.

Spectral vegetation indices used to estimate biophysical variables are usually developed to detect changes in the physical or chemical composition of leaves based on narrow-band optical properties (Zarco-Tejada et al., 2001). The scaling-up of these results is not always feasible because of the heterogeneity and geometry of the crown. In fact, this study demonstrates that most of the spectral indices related to $Cx+c$ content at leaf level were not directly applicable to the higher spatial scale of the crown. These results agree with previous studies that have highlighted the need to assess the structural and viewing geometry effects to properly scale-up physiological indices from leaf to crown level (Meggio et al., 2010; Suárez et al., 2008).

5. Conclusions

This study highlights that traditional vegetation indices related to $Cx+c$ content behave differently at the leaf and at crown level based

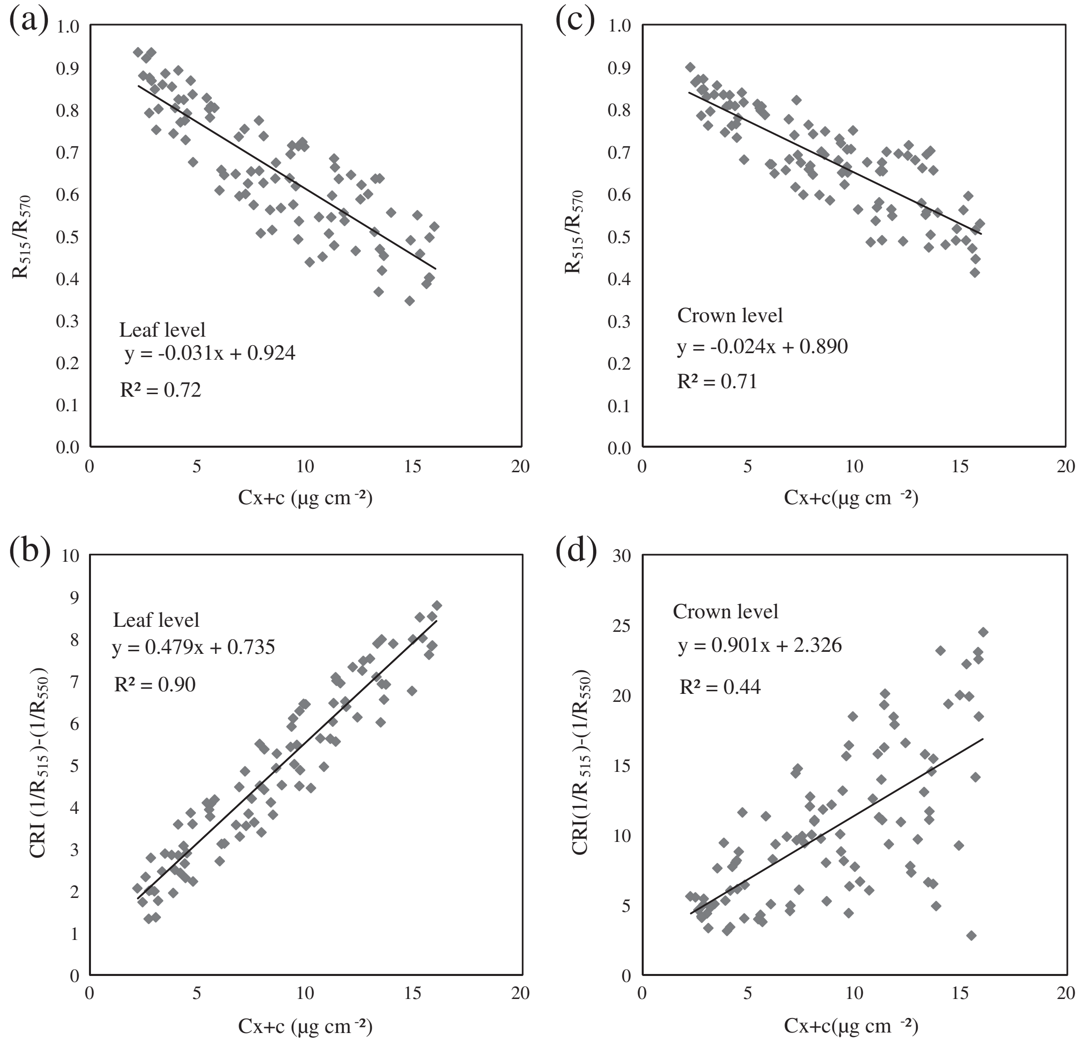

Fig. 9. Relationships obtained between $Cx+c$ and vegetation indices R_{515}/R_{570} (a) and CRI $(1/R_{515})-(1/R_{550})$ (b) at leaf level and crown level (c) and (d). Simulations conducted considering random variation of leaf $Cx+c$ (2–16 μg cm^{-2}) and $Ca+b$ (10–60 μg cm^{-2}) for crown LAI ranging between 1 and 8.

on radiative transfer modeling and field and airborne data validation. The study was conducted in a conifer forest, where structure plays an important role. The modeling simulation analysis showed that a new narrow-band vegetation index tested in this study (R_{515}/R_{570}) was sensitive to $Cx+c$ content variations at leaf level and was the most robust of all the indices at canopy level. The present study combined field, laboratory and modeling methods to assess the scaling-up of $Cx+c$-related vegetation indices to the canopy level. Results demonstrated that simple ratios formulated with bands R_{515} and R_{520} using reference bands R_{560} and R_{570} were sensitive to $Cx+c$ content at the leaf and crown level. In particular, index R_{515}/R_{570} showed the best relationship with $Cx+c$ at both leaf and canopy levels and was the least affected by the canopy structure. The robustness of other indices at leaf level was highly correlated to LAI and tree density values at crown level. The results obtained in this study show that at stand level, relationships between the spectral response and leaf chemistry tend to break down due to confounding factors related to the structure of the crown and background contributions.

Simulation results were in agreement with empirical results obtained at leaf and crown levels. The use of narrow-band multispectral cameras on board UAV platforms made it possible to validate this study and obtain high-resolution image data to map biophysical variables. These results demonstrate the feasibility of estimating $Cx+c$ with narrow-band multispectral imagery and confirm the findings obtained by modeling methods.

Acknowledgments

Financial support was provided by the GESBOME project (Regional Andalusian Government P06-RNN-1890). Support from the Spanish Ministry of Science and Education (MEC) to the AGL2009-13105 project is gratefully acknowledged. We would like to thank D. Notario, A. Vera, A. Hornero, R. Romero, L. Suárez and J.A.J. Berni for their technical support during field and UAV airborne campaigns. We are also grateful to J. E. Granados and the members of CAHA (German–Spanish Astronomical Center at Calar Alto), R. Sanchez (ERSAF), D. Ariza (IDAF), E. Gil-Pelegrín and J. J. Peguero-Pina (CITA, Zaragoza) for providing technical support during the fieldwork campaigns. Finally, we greatly appreciate the support of J. P. Gastellu-Etchegorry with the DART 3D radiative transfer model.

References

Abadía, A., & Abadía, J. (1993). Iron and plant pigments. In L. L. Barton, & B. C. Hemming (Eds.), *Iron chelation in plants and soil microorganisms* (pp. 327–344). San Diego: Academic.

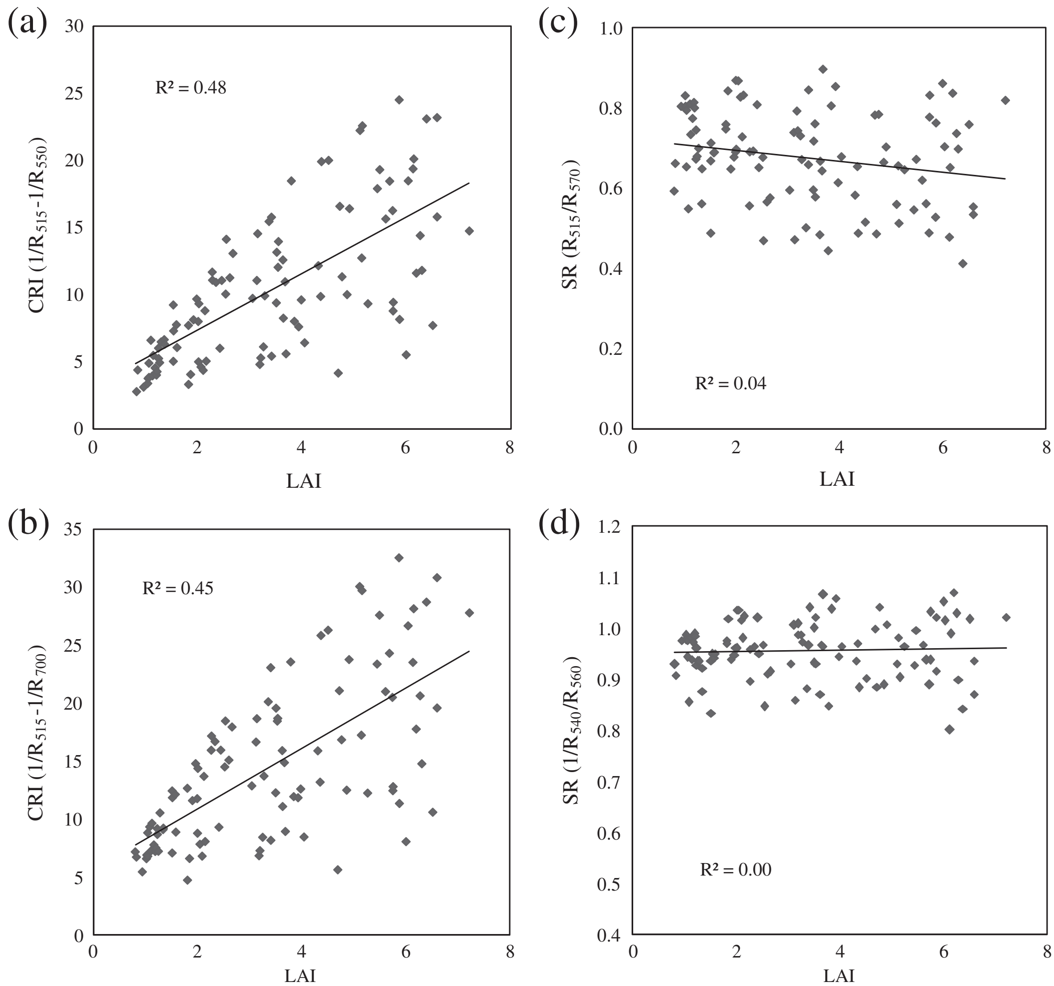

Fig. 10. Crown-level simulations performed with PROSPECT-5 leaf model coupled with DART considering random leaf *Cx* + *c* (2–16 μg cm^{-2}) and *Ca* + *b* (10–60 μg cm^{-2}) values and LAI ranging between 1 and 8 to assess the effects of the canopy density variation on indices $(1/R_{515})-(1/R_{550})$ (a), $(1/R_{515})-(1/R_{700})$ (b), (R_{515}/R_{570}) (c) and (R_{520}/R_{570}) (d).

Ardila, J. P., Bijker, W., Tolpekin, V. A., & Stein, A. (2012). Context-sensitive extraction of tree crown objects in urban areas using VHR satellite images. *International Journal of Applied Earth Observation and Geoinformation*, *15*, 57–69.

Berni, J. A. J., Zarco-Tejada, P. J., Sepulcre-Cantó, G., Fereres, E., & Villalobos, F. J. (2009). Mapping canopy conductance and CWSI in olive orchards using high resolution thermal remote sensing imagery. *Remote Sensing of Environment*, *113*, 2380–2388.

Blackburn, G. A. (1998). Quantifying chlorophylls and carotenoids at leaf and canopy scales: An evaluation of some hyperspectral approaches. *Remote Sensing of Environment*, *66*, 273–285.

Broge, N. H., & Leblanc, E. (2001). Comparing prediction power and stability of broadband and hyperspectral vegetation indices for estimation of green leaf area index and canopy chlorophyll density. *Remote Sensing of Environment*, *76*, 156–172.

Carter, G. A. (1994). Ratios of leaf reflectances in narrow wavebands as indicators of plant stress. *International Journal of Remote Sensing*, *15*, 697–704.

Carter, G. A., & Spiering, B. A. (2002). Optical properties of intact leaves for estimating chlorophyll content. *Journal of Environmental Quality*, *31*, 1424–1432.

Chappelle, E. W., Kim, M. S., & McMurtrey, J. E., III (1992). Ratio analysis of reflectance spectra (RARS): An algorithm for the remote estimation of the concentrations of chlorophyll a, chlorophyll b, and carotenoids in soybean leaves. *Remote Sensing of Environment*, *39*, 239–247.

Datt, B. (1998). Remote sensing of chlorophyll a, chlorophyll b, chlorophyll a + b, and total carotenoid content in Eucalyptus leaves. *Remote Sensing of Environment*, *66*, 111–121.

Demmig-Adams, B., & Adams, W. W., III (1992). Photoprotection and other responses of plants to high light stress. *Annual Review of Plant Physiology and Plant Molecular Biology*, *43*, 599–626.

Demmig-Adams, B., & Adams, W. W. (1996). The role of xanthophyll cycle carotenoids in the protection of photosynthesis. *Trends in Plant Science*, *1*, 21–26.

Faria, T., García-Plazaola, J. I., Abadia, A., Cerasoli, S., Pereira, J. S., & Chaves, M. M. (1996). Diurnal changes in photoprotective mechanisms in leaves of cork oak (*Quercus suber*) during summer. *Tree Physiology*, *16*, 115–123.

Féret, J. B., François, C., Asner, G. P., Gitelson, A. A., Martin, R. E., Bidel, L. P. R., et al. (2008). PROSPECT-4 and 5: Advances in the leaf optical properties model separating photosynthetic pigments. *Remote Sensing of Environment*, *112*, 3030–3043.

Féret, J. B., François, C., Gitelson, A., Asner, G. P., Barry, K. M., Panigada, C., et al. (2011). Optimizing spectral indices and chemometric analysis of leaf chemical properties using radiative transfer modeling. *Remote Sensing of Environment*, *115*, 2742–2750.

Frank, H. A., & Cogdell, R. J. (1996). Carotenoids in photosynthesis. *Photochemistry and Photobiology*, *63*, 257–264.

Gamon, J. A., Peñuelas, J., & Field, C. B. (1992). A narrow-wave band spectral index that tracks diurnal changes in photosynthetic efficiency. *Remote Sensing of Environment*, *41*, 35–44.

Garrity, S. R., Eitel, J. U. H., & Vierling, L. A. (2011). Disentangling the relationships between plant pigments and the photochemical reflectance index reveals a new approach for remote estimation of carotenoid content. *Remote Sensing of Environment*, *115*, 628–635.

Gastellu-Etchegorry, J. P., & Bruniquel-Pinel, V. (2001). A modeling approach to assess the robustness of spectrometric predictive equations for canopy chemistry. *Remote Sensing of Environment*, *76*, 1–15.

Gastellu-Etchegorry, J. P., Demarez, V., Pinel, V., & Zagolski, F. (1996). Modeling radiative transfer in heterogeneous 3-D vegetation canopies. *Remote Sensing of Environment*, *58*, 131–156.

Gastellu-Etchegorry, J. P., Martin, E., & Gascon, F. (2004). DART: A 3D model for simulating satellite images and studying surface radiation budget. *Internation Journal of Remote Sensing*, *25*, 73–96.

Gitelson, A. A., Gritz, U., & Merzlyak, M. N. (2003). Relationships between leaf chlorophyll content and spectral reflectance and algorithms for non-destructive chlorophyll assessment in higher plant leaves. *Journal of Plant Physiology*, *160*, 271–282.

Gitelson, A. A., Keydan, G. P., & Merzlyak, M. N. (2006). Three-band model for noninvasive estimation of chlorophyll, carotenoids, and anthocyanin content in higher plant leaves. *Geophysical Research Letters*, *33*, L11402.

Gitelson, A. A., & Merzlyak, M. N. (1996). Signature analysis of leaf reflectance spectra: Algorithm development for remote sensing of chlorophyll. *Journal of Plant Physiology*, *148*, 494–500.

Gitelson, A. A., Zur, Y., Chivkunova, O. B., & Merzlyak, M. N. (2002). Assessing carotenoid content in plant leaves with reflectance spectroscopy. *Journal of Photochemistry and Photobiology B-Biology*, *75*, 272–281.

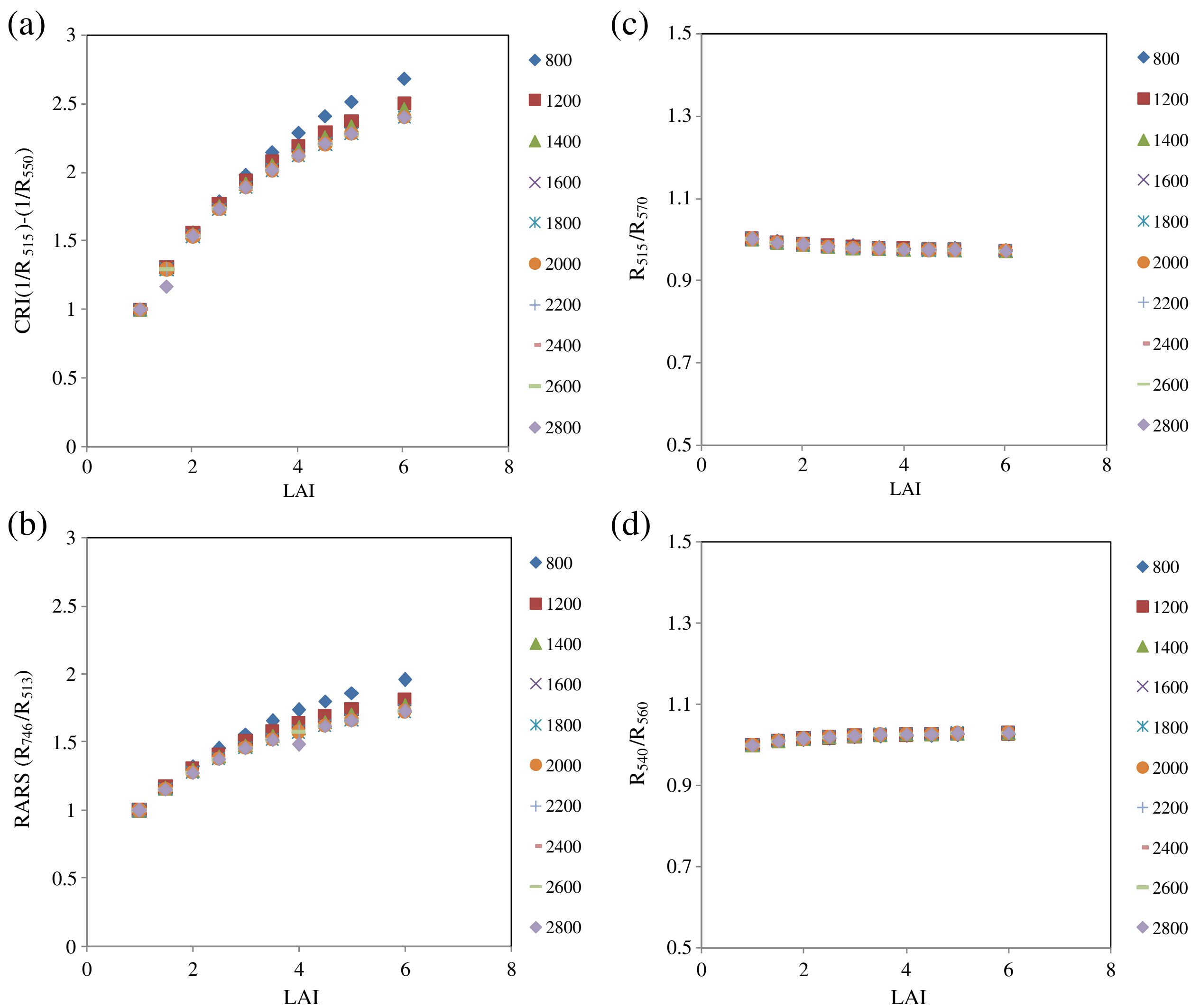

Fig. 11. Canopy-level model simulations conducted with PROSPECT-5 coupled with DART to assess the effect of the $Cx+c$ and $Ca+b$ content variations on indices used for $Cx+c$ estimation such as $(1/R_{515})-(1/R_{550})$ (a), (R_{746}/R_{513}) (b), (R_{515}/R_{570}) (c) and (R_{540}/R_{560}) (d). Simulations were performed for LAI ranging 1–6 and tree density variations from 800 to 2800 trees ha^{-1}. Values are normalized to LAI = 1.

Gueymard, C. A. (1995). *SMARTS, a simple model of the atmospheric radiative transfer of sunshine: Algorithms and performance assessment.* Technical Report No. FSECPF-270–95. Cocoa, FL: Florida Solar Energy Center.

Gueymard, C. A. (2001). Parameterized transmittance model for direct beam and circumsolar spectral irradiance. *Solar Energy*, *71*, 325–346.

Haboudane, D., Miller, J. R., Tremblay, N., Zarco-Tejada, P. J., & Dextraze, L. (2002). Integrated narrow-band vegetation indices for prediction of crop chlorophyll content for application to precision agriculture. *Remote Sensing of Environment*, *81*, 416–426.

Hernández-Clemente, R., Navarro-Cerrillo, R. M., Suárez, L., Morales, F., & Zarco-Tejada, P. J. (2011). Assessing structural effects on PRI for stress detection in conifer forests. *Remote Sensing of Environment*, *115*, 2360–2375.

Jacquemoud, S., & Baret, F. (1990). PROSPECT: A model of leaf optical properties spectra. *Remote Sensing of Environment*, *34*, 75–91.

Kirchgebner, H. D., Reichert, K., Hauff, K., Steinbrcher, R., Schnitzler, J. P., & Pfündel, E. E. (2003). Light and temperature, but not UV radiation, affect chlorophylls and carotenoids in Norway spruce needles (*Picea abies* (L.) Karst.). *Plant, Cell & Environment*, *26*, 1169–1179.

Kurtz, C., Passat, N., Gançarski, P., & Puissant, A. (2012). Extraction of complex patterns from multiresolution remote sensing images: A hierarchical top–down methodology. *Pattern Recognition*, *45*, 685–706.

Larbi, A., Abadía, A., Morales, F., & Abadía, J. (2004). Fe resupply to Fe-deficient sugar beet plants leads to rapid changes in the violaxanthin cycle and other photosynthetic characteristics without significant de novo chlorophyll synthesis. *Photosynthesis Research*, *79*, 59–69.

le Maire, G., François, C., & Dufrêne, E. (2004). Towards universal broad leaf chlorophyll indices using PROSPECT simulated database and hyperspectral reflectance measurements. *Remote Sensing of Environment*, *89*, 1–28.

Lichtenhaler, H. K. (1998). The stress concept in plants: An introduction. *Annals of the New York Academy of Sciences*, *851*, 187–198.

Main, R., Cho, M. A., Mathieu, R., O'Kennedy, M. M., Ramoelo, A., & Koch, S. (2011). An investigation into robust spectral indices for leaf chlorophyll estimation. *ISPRS Journal of Photogrammetry and Remote Sensing*, *66*, 751–761.

Malenovsky, Z., Homolova, L., Cudlin, P., Zurita-Milla, R., Schaepman, M. E., Clevers, J. G. P. W., et al. (2007). Physically-based retrievals of Norway spruce canopy variables from very high spatial resolution hyperspectral data. *Proc. IEEE International Geoscience and Remote Sensing Symposium (IGARSS'07), Barcelona, Spain*.

Malenovsky, Z., Martinb, E., Homolovác, L., Gastellu-Etchegorry, J. P., Zurita-Milla, R., Schaepman, M. E., et al. (2008). Influence of woody elements of a Norway spruce canopy on nadir reflectance simulated by the DART model at very high spatial resolution. *Remote Sensing of Environment*, *112*, 1–18.

Meggio, F., Zarco-Tejada, P. J., Miller, J. R., Martín, P., González, M. R., & Berjón, A. (2008). Row orientation and viewing geometry effects on row-structured vine crops for chlorophyll content estimation. *Canadian Journal of Remote Sensing*, *34*, 220–234.

Meggio, F., Zarco-Tejada, P. J., Núñez, L. C., Sepulcre-Cantó, G., Gonzalez, M. R., & Martin, P. (2010). Grape quality assessment in vineyards affected by iron deficiency chlorosis using narrow-band physiological remote sensing indices. *Remote Sensing of Environment*, *114*, 1968–1986.

Merzlyak, M. N., Gitelson, A. A., Chivkunova, O. B., & Rakitin, V. Y. (1999). Non-destructive optical detection of leaf senescence and fruit ripening. *Physiologia Plantarum*, *106*, 135–141.

Miller, J. R., Hare, E. W., & Wu, J. (1990). Quantitative characterization of the vegetation red edge reflectance. An inverted-Gaussian reflectance model. *International Journal of Remote Sensing*, *11*, 1755–1773.

Moorthy, I., Miller, J. R., & Noland, T. L. (2008). Estimating chlorophyll concentration in conifer needles with hyperspectral data: An assessment at the needle and canopy level. *Remote Sensing of Environment*, *112*, 2824–2838.

Munné-Bosch, S., & Peñuelas, J. (2003). Photo- and antioxidative protection, and a role for salicylic acid during drought and recovery in field-grown *Phillyrea angustifolia* plants. *Planta*, *217*, 758–766.

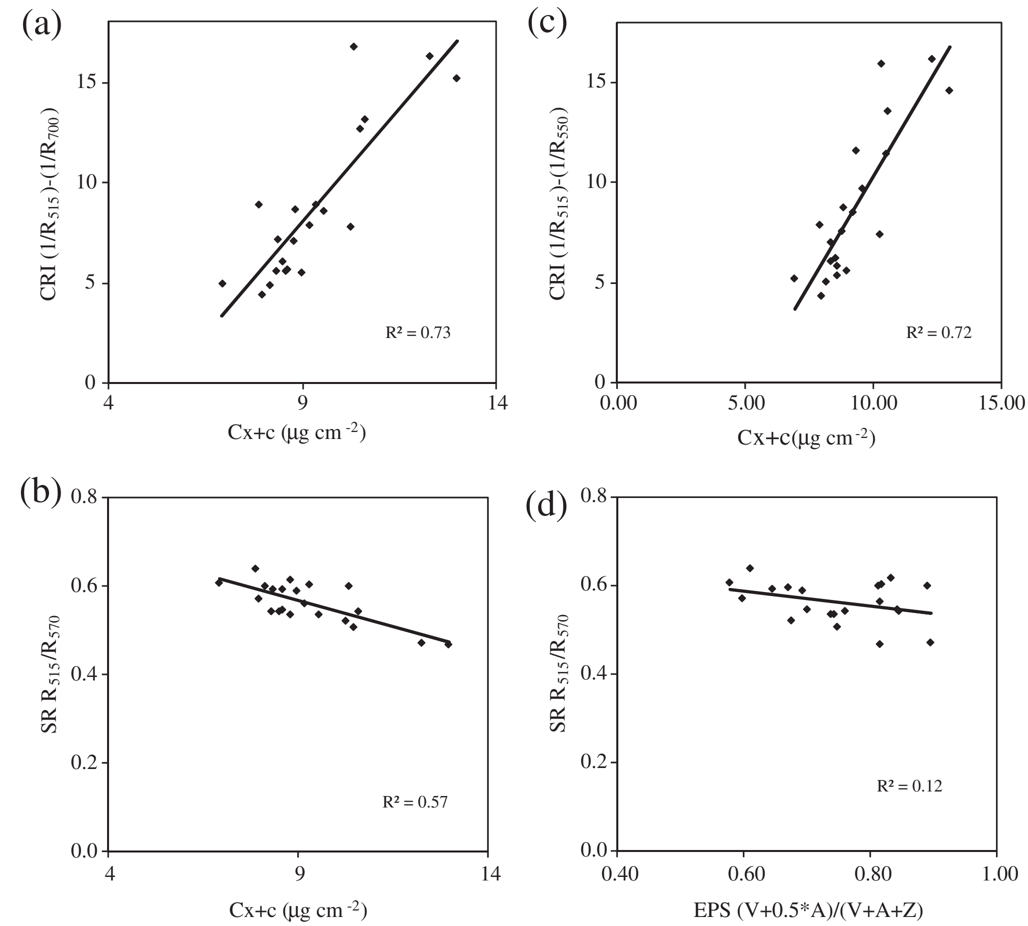

Fig. 12. Relationships between $Cx+c$ content and the following indices: Gitelson $(1/R_{515})-(1/R_{700})$ (a), simple ratio index (R_{515}/R_{570}) (b) and Gitelson $(1/R_{515})-(1/R_{550})$ (c). Relationships obtained between EPS and the simple ratio index (R_{515}/R_{570}) (d). Results obtained from leaf-level measurements.

Peñuelas, J., Baret, F., & Filella, I. (1995). Semi-empirical indices to assess carotenoids/chlorophyll a ratio from leaf spectral reflectance. *Photosynthetica*, *31*, 221–230.

Peñuelas, J., Gamon, J., Freeden, A., Merino, J., & Field, C. (1994). Reflectance indices associated with physiological changes in nitrogen- and water-limited sunflower leaves. *Remote Sensing of Environment*, *48*, 135–146.

Pinty, B., Gobron, N., Widlowski, J. L., Gerstl, S. A. W., Vertraete, M. M., Antunes, M., et al. (2001). Radiation transfer model intercomparison (RAMI) exercise. *Journal of Geophysical Research*, *106*, 11937–11956.

Richardson, A. D., & Berlyn, P. (2002). Changes in foliar spectral reflectance and chlorophyll fluorescence of four temperate species following branch cutting. *Tree Physiology*, *22*, 499–506.

Ritz, T., Damjanovic, A., Schulten, K., Zhang, J. P., & Koyama, Y. (2000). Understanding efficient light-harvesting through carotenoids with novel theoretical and experimental techniques. *Photosynthesis Research*, *66*, 125–144.

Rondeaux, G., Steven, M., & Baret, F. (1996). Optimization of soil-adjusted vegetation indices. *Remote Sensing of Environment*, *55*, 95–107.

Rouse, J. W., Haas, R. H., Schell, J. A., Deering, D. W., & Harlan, J. C. (1974). *Monitoring the vernal advancement and retrogradation (greenwave effect) of natural vegetation.* Type III Final Report. Greenbelt, Maryland, 20771, USA: NASA Goddard Space Flight Center 371 pp.

Sims, D. A., & Gamon, J. A. (2002). Relationships between leaf pigment content and spectral reflectance across a wide range of species, leaf structures and developmental stages. *Remote Sensing of Environment*, *81*, 337–354.

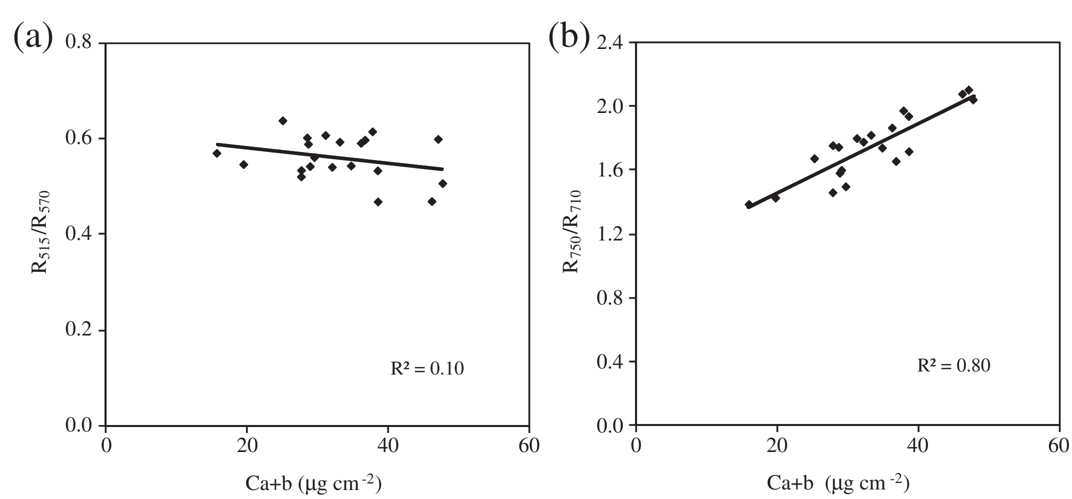

Fig. 13. Relationships obtained between R_{515}/R_{570} (a) and R_{750}/R_{710} (b) when compared to $Ca+b$ content. Results obtained from leaf-level measurements.

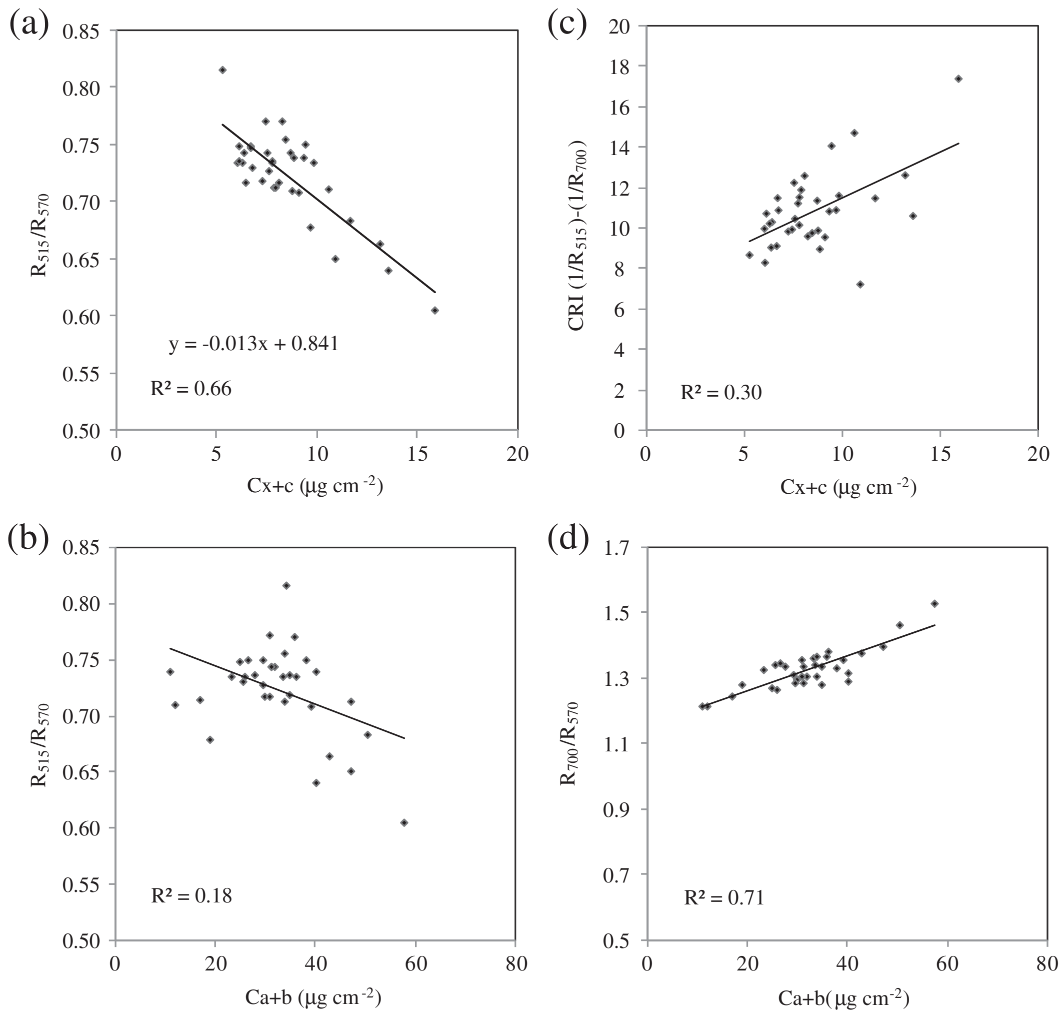

Fig. 14. Relationships obtained between $Cx+c$ (a, c) and $Ca+b$ contents (b, d) when compared to vegetation indices R_{515}/R_{570} (a, b), CRI_{700} (c) and R_{700}/R_{570} (d). Indices calculated at canopy level from the high-resolution multispectral camera on board the UAV platform.

Suárez, L., Zarco-Tejada, P. J., Berni, J. A. J., González-Dugo, V., & Fereres, E. (2009). Modelling PRI for water stress detection using radiative transfer models. *Remote Sensing of Environment*, *113*, 730–744.

Suárez, L., Zarco-Tejada, P. J., González-Dugo, V., Berni, J. A. J., Sagardoy, R., Morales, F., et al. (2010). Detecting water stress effects on fruit quality in orchards with time-series PRI airborne imagery. *Remote Sensing of Environment*, *114*, 286–298.

Suárez, L., Zarco-Tejada, P. J., Sepulcre-Cantó, G., Pérez-Priego, O., Miller, J. R., Jiménez-Muñoz, J. C., et al. (2008). Assessing canopy PRI for water stress detection with diurnal airborne imagery. *Remote Sensing of Environment*, *112*, 560–575.

Thayer, S. S., & Björkman, O. (1990). Leaf xanthophyll content and composition in sun and shade determined by HPLC. *Photosynthesis Research*, *23*, 331–343.

Widlowski, J. L., Taberner, M., Pinty, B., Bruniquel-Pinel, V., Disney, M., Fernandes, R., et al. (2007). Third Radiation Transfer Model Intercomparison (RAMI) exercise: Documenting progress in canopy reflectance models. *Journal of Geophysical Research*, *112*, D09111.

Wu, S. L., Mickley, L. J., Jacob, D. J., Rind, D., & Streets, D. G. (2008). Effects of 2000–2050 changes in climate and emissions on global tropospheric ozone and the policy-relevant background surface ozone in the United States. *Journal of Geophysical Research*, *108*, D18312.

Young, A., & Britton, G. (1990). Carotenoids and stress. In R. G. Alscher, & J. R. Cumming (Eds.), *Stress responses in plants: Adaptation and acclunation mechanisms* (pp. 87–112). New York: Wiley- Liss.

Young, A. J., Phillip, D., & Savill, J. (1997). Carotenoids in higher plant photosynthesis. In M. Pessaraki (Ed.), *Handbook of photosynthesis* (pp. 575–596). New York: Marcel Dekker.

Zarco-Tejada, P. J., Berni, J. A. J., Suárez, L., Sepulcre-Cantó, G., Morales, F., & Miller, J. R. (2009). Imaging chlorophyll fluorescence from an airborne narrow-band multispectral camera for vegetation stress detection. *Remote Sensing of Environment*, *113*, 1262–1275.

Zarco-Tejada, P. J., González-Dugo, V., & Berni, J. A. J. (2012). Fluorescence, temperature and narrow-band indices acquired from a UAV platform for water stress detection using a micro-hyperspectral imager and a thermal camera. *Remote Sensing of Environment*, *117*, 322–337.

Zarco-Tejada, P. J., Miller, J. R., Harron, J., Hu, B., Noland, T. L., Goel, N., et al. (2004). Needle chlorophyll content estimation through model inversion using hyperspectral data from boreal conifer forest canopies. *Remote Sensing of Environment*, *89*, 189–199.

Zarco-Tejada, P. J., Miller, J. R., Mohammed, G. H., Noland, T. L., & Sampson, P. H. (2001). Scaling-up and model inversion methods with narrow-band optical indices for chlorophyll content estimation in closed forest canopies with hyperspectral data. *IEEE Transactions on Geoscience and Remote Sensing*, *39*, 1491–1507.

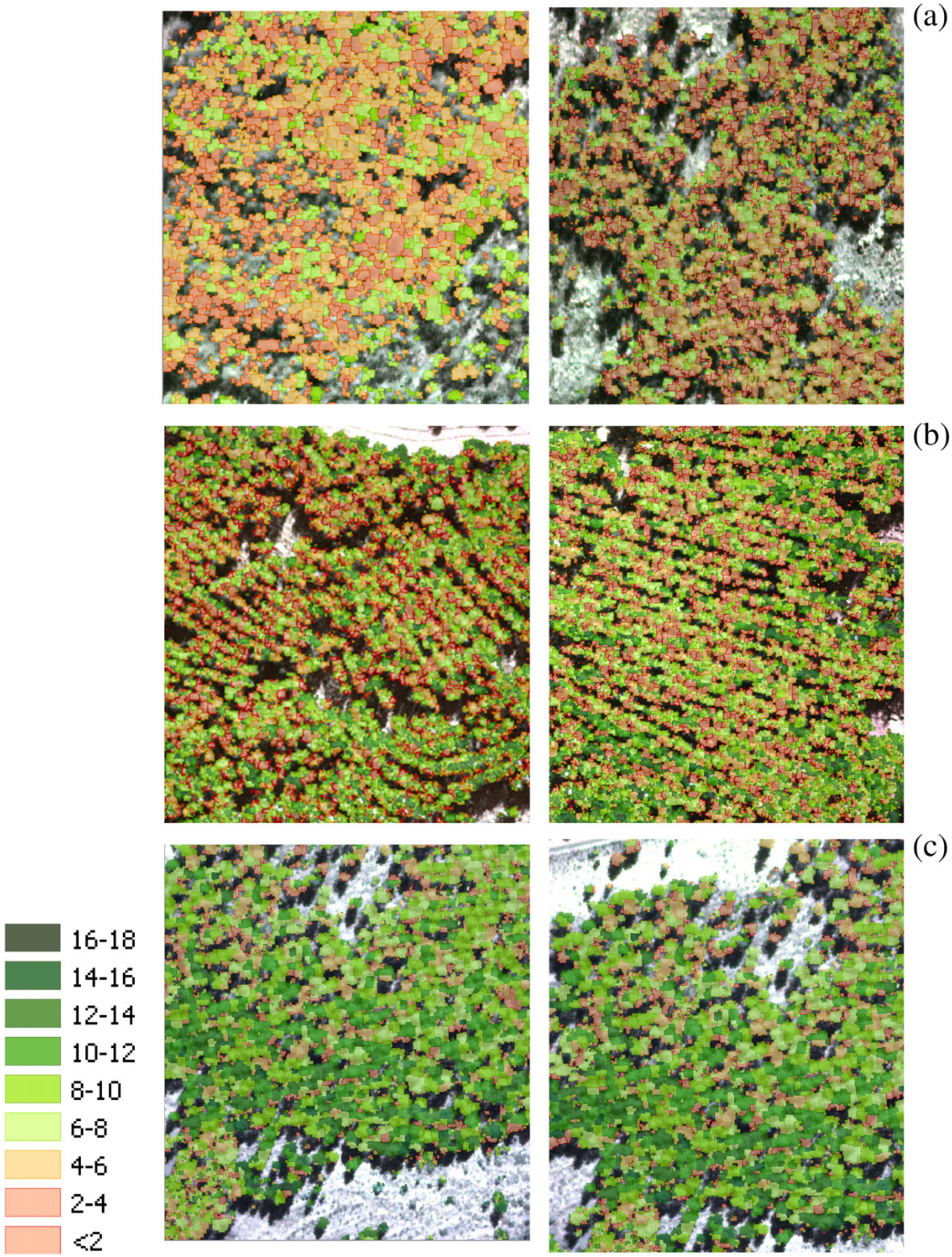

Fig. 15. Maps showing the spatial variation of $Cx+c$ content μg cm^{-2} using the index R_{515}/R_{570} through scaling-up. Imagery acquired with the narrow-band multispectral camera on board the UAV platform. Maps with different mean values of carotenoid content are shown for 2–6 μg cm^{-2} (a), 6–12 μg cm^{-2}(b), and 12–18 μg cm^{-2} (c).